Available online at www.sciencedirect.com
SCIENCE DIRECT®
Journal of Catalysis 221 (2004) 630–649
JOURNAL OF CATALYSIS
www.elsevier.com/locate/jcat

Microkinetic modeling of ethylene oxidation over silver

C. Stegelmann,[a] N.C. Schiødt,[b] C.T. Campbell,[c] and P. Stoltze [a,*]

[a] *Department of Chemistry and Applied Engineering Science, Aalborg University, Niels Bohrs Vej 8 DK-6700 Esbjerg, Denmark*
[b] *Haldor Topsøe A/S, Nymøllevej 55, DK-2800 Lyngby, Denmark*
[c] *Department of Chemistry, University of Washington, Seattle, WA 98195-1700, USA*

Received 16 July 2003; revised 26 September 2003; accepted 3 October 2003

Abstract

In the present work a detailed microkinetic model based on the surface science of ethylene oxidation over silver has been developed. The active phase of the catalyst is suggested to be a surface oxide on which atomic oxygen and ethylene can adsorb and react to form an oxametallacycle. The oxide oxygen creates $Ag^{\delta+}$ sites which promotes the adsorption of ethylene and is often termed nucleophilic or ionic oxygen in the literature. A less stable atomic oxygen often referred to as electrophilic or covalent in the literature is suggested to compete with ethylene for the $Ag^{\delta+}$ sites. The oxametallacycle is a common intermediate in epoxidation, ethylene combustion, and ethylene oxide combustion. The microkinetic model reproduces experimental heats of adsorption, sticking, TPD, and TPR measurements. The kinetics of epoxidation, ethylene combustion, and ethylene oxide combustion has been simulated by the model. The model has been validated successfully by comparing model output to measured initial rates for both oxygen- and ethylene-rich mixtures at different temperatures. Selectivity, apparent activation energies, isotope effects, and reaction orders are reproduced by the model. The rate and selectivity controlling steps in the reaction mechanism and the critical parameters of the model have been identified.

Keywords: Ethylene epoxidation; Selectivity; Silver; Microkinetic modeling; Partial oxidation

1. Introduction

Since the work of Lefort, ethylene oxide has been produced almost exclusively by partial oxidation of ethylene over a silver catalyst [1,2]. This reaction is *one* of the major petrochemical processes converting several billion US dollars annually due to the importance of ethylene oxide as a versatile chemical intermediate [1,2]. The kinetics of ethylene oxidation on silver is traditionally described by the net reactions [1–7]:

$$C_2H_4 + \tfrac{1}{2}O_2 \rightleftharpoons C_2H_4O, \quad (1)$$

$$C_2H_4 + 3O_2 \rightleftharpoons 2CO_2 + 2H_2O, \quad (2)$$

$$C_2H_4O + \tfrac{5}{2}O_2 \rightleftharpoons 2CO_2 + 2H_2O. \quad (3)$$

The chemical equilibrium strongly favors the formation of total oxidation products. The reason ethylene oxide is not further oxidized is purely kinetic. For both economic and technical reasons there has been great interest in increasing selectivity toward ethylene oxide and thereby reducing ethylene consumption and heat production. The improvement of 1% selectivity is estimated to produce a beneficial effect of several tens of million dollars annually [8]. The selectivity on unpromoted silver is about 40–50% while it is 80–85% on an optimized alkali and chlorine promoted commercial catalyst [1–3]. In the last 2–3 decades research has been continued in an effort to improve the selectivity further by optimizing the catalyst and the process conditions. However, the success of this effort has been limited and the selectivity has been stagnant. Early mechanistic studies summarized in the famous "6/7 rule" even suggested that an upper theoretical selectivity limit of 85.7% exists [1,2,9]. Recent surface science studies and reported selectivities above 85.7% disprove the 6/7 rule [3,10]. It is very important to establish what limits the selectivity of ethylene epoxidation and if/how it is possible to optimize the selectivity further. In order to do so a detailed reaction mechanism of ethylene epoxidation and combustion is needed. However, despite the fact that ethylene oxidation on silver has been extensively studied by both experimental and theoretical methods the reaction mechanism remains controversial.

* Corresponding author.
E-mail address: stoltze@aue.auc.dk (P. Stoltze).

0021-9517/$ – see front matter
doi:10.1016/j.jcat.2003.10.004

In fact, ethylene epoxidation is the most studied partial oxidation to date and almost every conceivable experiment has been performed for this reaction. A powerful way to systematically investigate the vast amount of experimental data and develop a consistent reaction mechanism of ethylene oxidation on silver is the use of microkinetic analysis and modeling [11,12]. A successful microkinetic model should be able to close the pressure, temperature, and material gaps between experimental and theoretical surface science and industrial catalysis. Furthermore, a successful microkinetic model gives the opportunity to understand the critical aspects of activity and selectivity and guide future research.

Industrial ethylene epoxidation is performed in a cooled shell-and-tube recycle reactor with a contact time of approximately 1 s [1,2]. The temperature and pressure are 473–573 K and 1–3 MPa, respectively. For the desired high selectivity the conversion is held at 10–15% per pass. Using industrial grade oxygen, the feed comprised of fresh feed mixed with recycled gas consists typically of about 20 vol% ethylene, 6–8 vol% oxygen, 6 vol% CO_2, 4–5 vol% Ar, the remainder being nitrogen and methane. The catalyst consists of 10–18 wt% silver dispersed on low area α-Al_2O_3. The alumina is low area presumably to provide large pores and avoid the diffusion-limited regime that would reduce selectivity [1,2]. The catalyst is promoted by alkali metals and chlorine is continuously added during the reaction, thereby increasing selectivity. The major challenges of the process are heat removal and avoidance of explosions [1,2].

There are many features of ethylene epoxidation that have puzzled scientists for decades. Surprisingly, silver is an exceptional catalyst material for ethylene epoxidation. To the best of our knowledge no other material comes even close to producing the epoxidation activity and selectivity of silver under practical conditions. However, Lambert and co-workers [13,14] have shown that in UHV copper is an even more selective epoxidation catalyst than silver. Unfortunately, an inactivating oxide overlayer is formed on copper in the presence of gas-phase oxygen [13,14]. The reasons for the limited selectivity are also unknown and it is in particular unknown if and how it is possible to increase the selectivity further. Only ethylene of the simple alkenes undergo epoxidation, while a compound such as propylene combusts. However, epoxides derived from higher alkenes without allylic hydrogen such as norborene, styrene, and butadiene may be produced by partial oxidation with high selectivity [15–18]. The role of alkali and chlorine as selectivity promoters also remains unknown. Many scientists believe that the interaction between oxygen and silver plays an essential role in understanding ethylene epoxidation and a great research effort has been devoted to the silver–oxygen system [3,19]. However, the form and the creation of the active oxygen species are still debated.

It has not been possible to study ethylene epoxidation directly in UHV by surface science techniques, presumable because ethylene and/or the active oxygen species desorbs before the reaction barrier can be climbed. This is probably the main reason that the mechanism remains controversial. However, intermediates such as molecular oxygen [20,21], atomic oxygen [20,22–27], subsurface/dissolved oxygen [28–30], ethylene [31–33], ethylene oxide [31,34–36], acetaldehyde [37], water [38], carbon dioxide [39], and oxametallacycles [40,41] have been studied by surface science techniques. Furthermore, the reactions of intermediates have been studied by a number of transient techniques, such as TPR [28,29,42–46], pulse reactors [47–49], batch reactors [6,43], and combining high-pressure cells with UHV techniques [42,50,51].

The kinetics of ethylene epoxidation and combustion have been studied extensively by a number of authors [4–7, 42,43,49–62]. To the best of our knowledge, a single kinetic expression that reproduces the kinetics for both ethylene-rich and oxygen-rich feeds does not exist. Instead different kinetic expressions are used for different reaction conditions. This indicates a very complicated kinetics for this process. The most favored kinetic expressions in the literature seem to be of the competitive Langmuir–Hinshelwood type [53,54,59]. One of the more important kinetic findings is that both epoxidation and combustion display similar trends for apparent activation energies and reaction orders in ethylene and oxygen pressure, respectively [50,51,53–55,60]. Reaction orders in oxygen can exceed one at low oxygen pressures and decrease to negative values for very high oxygen pressures [53,54]. Reaction orders in ethylene have a value of approximately one at low ethylene pressure and become negative at high ethylene pressure [53,54]. Maxima in the activity of epoxidation and combustion have therefore been observed as a function of both ethylene and oxygen pressure. Apparent activation energies of epoxidation and combustion have been reported in the range 20–110 kJ/mol depending on reaction conditions [6,7,19,50,63]. The reaction orders in oxygen and ethylene of both epoxidation and combustion suggest that adsorbed ethylene and some adsorbed oxygen species compete for the same active sites. From reaction orders ethylene seems to compete more strongly for the active sites compared to the "active" oxygen species [50,51,53,54]. However, surface science indicates that ethylene is only weakly adsorbed on silver, while atomic oxygen adsorbs strongly in UHV [42].

Trends in selectivity are controversial in the literature. The majority of reports seem to indicate that selectivity decreases with temperature and increases with increasing O_2:C_2H_4 ratio [3,43,60]. However, opposite trends have also been reported [49–51,64]. Substituting the hydrogen in ethylene with deuterium results in a normal isotope effect for combustion; however, epoxidation increases unexpectedly with a large inverse isotope effect, resulting in a dramatic increase of the selectivity [42,55]. A similar effect has been observed for epoxidation of butadiene [16].

The older part of the literature is much concerned with the question of whether molecular or atomic adsorbed oxygen reacts with ethylene to form ethylene oxide [9,65]. Today experimental results indicate that atomic oxygen is the ac-

tive species [3]. Furthermore, it has been discussed if an Eley–Rideal or a Langmuir–Hinshelwood type of mechanism is appropriate to describe the process [3, and references therein].

Harriott and co-workers [53,54] and Temkin [62] suggested that the active phase of the catalyst was not metallic silver but a surface oxide. This explains the low stability of the active oxygen compared to ethylene, the increasing selectivity with O_2:C_2H_4 ratio, and the observed reaction orders greater than one.

Cant and Hall [55], Bell and Force [61], and Campbell and co-workers [50,51,66–68] suggested that epoxidation and combustion go through an unidentified common intermediate in the rate-limiting step. This mechanistic idea explains the similarities in kinetic trends of epoxidation and combustion. Furthermore, the model offers a very elegant explanation for the observed isotope effect [55,69]. Campbell suggested that molecular oxygen was active because experiments showed that the atomic oxygen in UHV could not be the active oxygen species [50,51,66–68]. For this reason the mechanism was largely abandoned, but recently Barteau and co-workers [40,69,70] and Tysoe and co-workers [41] demonstrated by a combined experimental surface science and DFT approach that oxametallacycles are likely common intermediates in both epoxidation and combustion. Linic and Barteau succeeded in making a microkinetic model for ethylene epoxidation based on a reaction coordinate calculated from first principles incorporating the oxametallacycle as a central intermediate [71]. A similar reaction coordinate has been calculated by King and co-workers [72] for both a metallic silver and a surface silver oxide.

Lambert and co-workers [42], van Santen and Kuipers [3], and Carter and Goddard [73] suggested that two different atomic oxygen species were active in epoxidation (electrophilic) and combustion (nucleophilic), respectively. Nucleophilic oxygen exists on clean silver, while electrophilic oxygen is created in the presence of subsurface oxygen and/or chlorine. This mechanism qualitatively explains a number of transient experiments. However, it is very difficult to interpret steady-state kinetics with this mechanism. Recently, Bal'zhinimaev modified the mechanism by suggesting that electrophilic oxygen is created on defect sites and not by subsurface oxygen [19, and references therein].

In the present work we will present a microkinetic model that describes ethylene epoxidation, ethylene combustion, and ethylene oxide combustion on unpromoted silver. The reaction mechanism and the parameters are mostly deduced explicitly from transient surface science experiments in UHV. In a few cases parameters are extracted from steady-state kinetics on single crystals. It is ensured that the parameters have physically realistic values. The model is validated by comparison with reported initial rates on different catalysts in a broad pressure and temperature region. A similar approach has recently been successfully applied to the related partial oxidation of methanol to formaldehyde on silver [74]. In general, microkinetic modeling has been successful in studying a number of important industrial reactions [11,12,75–83]. From a microkinetic model it is possible to estimate surface coverages, reaction orders, selectivity, apparent activation enthalpies, degree of rate control, etc. during reaction conditions. For this reason the applicability of the model is not restricted to a particular set of conditions, but can be used under various conditions where simplified models; e.g., power-law expressions may break down. In the present paper we will concentrate on the simulation of steady-state kinetics; however, the model is able to explain a broad range of transient experiments as well [84].

2. Methods

The starting point of a microkinetic model is a detailed reaction mechanism containing all the important elementary reactions. The principle of microscopic reversibility is applied to each elementary step, and the kinetics is described by Arrhenius expressions. A statistical mechanical description is used for all gas-phase molecules and adsorbates giving a correct description of the degrees of freedom for each species. Furthermore, statistic thermodynamics ensures a correct description of the gas-phase thermodynamics within the ideal gas approximation. The pivot in statistical mechanics is the partition function, and from this function all thermodynamic information can be extracted, e.g., the equilibrium constants for each step in the mechanism.

2.1. Reaction mechanism

In order to explain kinetic and surface science experiments a model containing both the ideas of a common intermediate [50,51,55,61,66–68] and an active surface oxide [53,54,62] is proposed. It should be noted that there is no general agreement in the literature about the existence of an active oxide layer or a common intermediate as illustrated in the Introduction. Especially, the formation of a surface oxide oxygen forming the active sites in epoxidation is speculative. The suggested detailed mechanism is depicted in Table 1. As shown in Table 1 and discussed below two sorts of active sites are suggested to exist, i.e., a metallic silver site (*) and some kind of surface oxide site (/O*). The exact configuration of the /O* site and the binding of intermediates to /O* are speculative. Hence we have used a "slash" notation to avoid any indications if intermediates are bonded to Ag, O, or both. /O* is simply a second type of active sites. However, it should be emphasized that the mechanism is not analyzed as a Horiuti–Polanyi mechanism, because the /O* sites are formed by a reaction between oxygen and silver. The mechanism is therefore analyzed as an ordinary Langmuir–Hinshelwood mechanism with one kind of active site (*). Furthermore, it should be stressed that it is implicitly

Table 1
Reaction mechanism for the microkinetic model

$O_2(g) + * \rightleftharpoons O_2^*$	(step 1)
$O_2^* + * \rightleftharpoons 2O^*$	(step 2)
$O_2(g) + 2O^* \rightleftharpoons 2O/O^*$	(step 3)
$C_2H_4(g) + O^* \rightleftharpoons C_2H_4/O^*$	(step 4)
$C_2H_4/O^* + O/O^* \rightleftharpoons CH_2CH_2O/O^* + O^*$	(step 5)
$C_2H_4O(g) + O^* \rightleftharpoons C_2H_4O/O^*$	(step 6)
$CH_2CH_2O/O^* \rightleftharpoons C_2H_4O/O^*$	(step 7)
$CH_2CH_2O/O^* \rightleftharpoons CH_3CHO/O^*$	(step 8)
$CH_3CHO/O^* \rightleftharpoons CH_3CHO(g) + O^*$	(step 9)
$CH_3CHO/O^* + 6O^* \rightleftharpoons 2CO_2^* + 4OH^* + *$	(step 10)
$C_2H_4(g) + * \rightleftharpoons C_2H_4{}^*$	(step 11)
$C_2H_4/O^* + O^* \rightleftharpoons CH_2CHOH/O^* + *$	(step 12)
$CH_2CHOH/O^* + O^* \rightleftharpoons CH_2CHO/O^* + OH^*$	(step 13)
$CH_2CHO/O^* + 5O^* \rightleftharpoons 2CO_2^* + 3OH^* + *$	(step 14)
$2OH^* \rightleftharpoons H_2O^* + O^*$	(step 15)
$CO_2^* \rightleftharpoons CO_2(g) + *$	(step 16)
$H_2O^* \rightleftharpoons H_2O(g) + *$	(step 17)

The asterisk signifies a metallic silver site, /O* is a surface oxide site, and X^* and Y/O* are an adsorbed species on metallic silver and surface oxide, respectively.

assumed that each O* forms one active site (/O*). This assumption might be incorrect; i.e., it is possible that each O* forms less or more than one active site. To answer this question more detailed modeling of the active sites is needed by such techniques as DFT, etc. However, we believe that the exact number of sites formed by O* is of minor importance and will not influence the overall conclusions of the present work. Further, as will become clear later it is assumed that one metallic silver site consists of two surface Ag atoms, which may not be the case in reality. In addition, it is implicitly assumed within the Langmuir–Hinshelwood treatment that interaction energies (coverage dependencies) are absent and that each intermediate only requires one metallic site (*). All of these assumptions may be questioned; however, the success of the microkinetic model demonstrated in the rest of this work shows that these assumptions are reasonable as a first approximation. It will in general not be possible to develop a microkinetic model without making certain initial assumptions or approximations.

The central idea of the mechanism is that dissociatively adsorption of O_2 or preadsorbed oxygen on metallic silver (O*) forms an surface oxide layer by reconstruction of the Ag surface (step 2). Such a reconstruction has been observed experimentally by LEED and STM [20,26,27] and by DFT calculations [85–87]. In particular, ab initio atomistic thermodynamic calculations have shown that the surface oxide layer is expected to be thermodynamically stable under industrial epoxidation conditions [85–87]. However, it will be shown later as a result of our microkinetic model that the formation of the surface oxide is limited by kinetics not thermodynamics. Epoxidation catalysts are therefore not covered with a surface oxide but are partly reduced in a reactive atmosphere of ethylene and oxygen. This reduction of the catalyst is explicitly built into the microkinetic model due to the participation of O* in the combustion of ethylene (steps 10, 12, 13, and 14).

O* is equivalent to the atomic surface oxygen observed in UHV also referred to as nucleophilic or ionic oxygen in the literature [3,19, and references therein]. On Ag(111), O* is the atomic surface oxygen observed to form a p(4 × 4)-O LEED pattern with XPS = 528.2 eV and desorbs at ∼580 K [20]. The equivalent O* on Ag(110) forms a c(6 × 2)-O LEED pattern with XPS = 528.1 eV and desorbs at ∼570 K [39]. The presence of O* results in a Ag $3d_{5/2}$ core level spectra equal to 367.6 eV in XPS, 0.5 eV less than that for the bulk metallic silver [88]. The coincidence of this value with that measured for silver oxides indicates the formation of Ag^+ ions [88]. We therefore refer to O* as a surface oxide in the following. The adsorption of O* is precursor mediated, with the precursor O_2^*, and goes through steps 1–2 in Table 1 [20,22]. We suggest that adsorbed ethylene (C_2H_4/O*) and another atomic oxygen species (O/O*) adsorb on the surface oxide (steps 3 and 4). By O/O* we mean an atomic oxygen atom (O) adsorbed on an surface oxide site (/O*); i.e., two O atoms are included in the O/O* symbol. We would like to emphasize that O/O* should not be confused for molecular adsorbed oxygen. Similarly, by C_2H_4/O* we mean ethylene (C_2H_4) adsorbed on a surface oxide site (/O*) and so forth for other intermediates adsorbed on surface oxide sites. The above proposal is consistent with experiments indicating that the number of active sites for ethylene epoxidation is proportional to the coverage of O*, which again is proportional to the sites for ethylene adsorption [19,50]. It is well known that ethylene adsorbs more strongly on silver containing preadsorbed oxygen [31–33, 42,50,66,89]. Some investigators even claim that ethylene cannot adsorb on reduced silver [42,89]. However, a more thorough investigation shows that ethylene adsorbs on both clean ($C_2H_4^*$ in step 11) and preoxidized silver (C_2H_4/O* in step 4), but with different binding energies [31,33,50,66]. This effect is suggested in the literature to be due to the formation of $Ag^{\delta+}$ sites created by O* [19,50,88–91]. The existence of atomic oxygen adsorbed on the surface oxide layer (O/O*) is more speculative. This species has not been identified in UHV studies probably due to desorption below 400 K. Most UHV studies concerning atomic oxygen on silver are performed above 400 K. Furthermore, the reconstruction of Ag(111) to form the surface oxide starts above 400 K [27,88]. However, from experiments it is well known that the heat of oxygen adsorption decreases dramatically above 0.5 ML coverage, which corresponds to the coverage of surface oxide [39,92,93]. This loosely bonded atomic oxygen is often referred to as electrophilic or covalent in the literature [3,19]. Interestingly, Scheffler and co-workers [94, and references therein] recently proposed a similar model for CO oxidation on RuO_2 based on DFT calculations. Here gas-phase oxygen creates an oxide with metallic Ru and another atomic surface oxygen adsorbs on the oxide structure, which is reactive in CO oxidation. In addition, Campbell and Paffett showed that going from p(2 × 1)-O (0.5 ML) to

c(6 × 2)-O (0.67 ML) on Ag(110) the heat of oxygen adsorption decreased ∼10% resulting in about 5 times more reactive oxygen for CO oxidation [39].

From the Introduction it is clear that the active oxygen in epoxidation has a low stability compared to atomic oxygen observed in UHV. Based on TPR experiments the formation of the loosely bonded electrophilic oxygen is often suggested to be promoted by the presence of subsurface oxygen in the literature [3,28,29,42,46]. However, if subsurface oxygen forms the loosely bonded surface oxygen necessary to explain reaction kinetics [51,53,54] and adsorption isotherms [92,93] a significant decrease in O* desorption temperature is expected in the presence of subsurface oxygen, which is not observed experimentally [28]. Furthermore, the formation of subsurface oxygen is slow and activated [42,95] and it is therefore doubtful that the uptake of subsurface oxygen is rapid enough to form the active sites necessary under steady-state conditions. Furthermore, Campbell and co-workers investigated steady-state kinetics on Ag(111) and Ag(110) in a high-pressure cell and rapidly transfered the single crystals to UHV after steady-state was obtained [50,51]. In these experiments only surface oxygen (O*) was observed after transfer to UHV even though subsurface oxygen should be even more thermally stable. This suggests that subsurface oxygen is unimportant under steady-state conditions. It is clear, however, that subsurface oxygen plays a role in the transient experiments of Grant and Lambert [42] and van Santen and co-workers [28,29]. We suggest that the role of subsurface oxygen in these transient experiments is to serve as an oxygen reservoir that supplies oxygen to the surface oxide. By including the elementary reactions

$$O^* + Ag_{subsurface} \rightleftharpoons O\text{–}Ag_{subsurface} + {}^*, \quad (4)$$

$$2O^* \rightleftharpoons O/O^* + {}^*, \quad (5)$$

in the model, the transient experiments of Grant and Lambert [42] and van Santen and co-workers [28,29] may be explained as demonstrated in a related paper [84].

In step 5 ethylene adsorbed on the surface oxide (C_2H_4/O*) reacts with electrophilic oxygen (O/O*) to form an oxametallacycle (CH_2CH_2O/O*), which is a common intermediate for both epoxidation and combustion. The oxametallacycle branches into either adsorbed ethylene oxide (C_2H_4O/O* in step 7) or acetaldehyde (CH_3CHO/O* in step 8). Experimental and theoretical evidence for a surface oxametallacycle incorporating two Ag atoms bonded to the O and C (Ag–CH_2CH_2O–Ag), respectively, has been reported [40,41]. Furthermore, it has been shown that this oxametallacycle can branch into ethylene oxide and acetaldehyde [40,69,70]. The rate ratio of steps 7 and 8 determines the selectivity. The adsorbed ethylene oxide desorbs (step 6) while acetaldehyde rapidly combusts (step 10) [6,7,57]. Step 10 is clearly not elementary; however, this combustion is very fast in the presence of oxygen and can be approximated as an elementary reaction with negligible error. It has been suggested that the combustion of acetaldehyde goes through acetate and formate intermediates [3,42]. In the absence of oxygen, adsorbed acetaldehyde will desorb to the gas phase instead of combusting (step 9) as observed experimentally [7,52,57].

The formed ethylene oxide combusts by isomerization to acetaldehyde through the oxametallacycle (steps 6–8), which is consistent with experiments [7,52,57]. Note that it is not necessary to include a new net reaction to explain ethylene oxide combustion. The isomerization of ethylene oxide to acetaldehyde and further oxidation (steps 6–10) can also proceed on metallic silver sites [57,96]. These steps are included in the model even though they are not shown in Table 1 for simplicity. These extra steps are only important for the further oxidation of ethylene oxide and only play a role under conditions where the oxide coverage is low. The parameters for the combustion of ethylene oxide on metallic sites are assumed to be identical to those on the oxide sites.

It is apparent from the mechanism that the formation of the oxametallacycle and adsorbed ethylene oxide does not necessitate the breaking of C–H bonds, while in the formation of acetaldehyde H has to migrate to another C atom. The model is therefore able to explain the large inverse isotope effect [55] in the way proposed by Linic and Barteau [69].

Ethylene also combusts through an alternative parallel pathway (steps 12–17), which is indicated by a number of experimental studies [42,46,50]. The details of this pathway are unknown, because it is very difficult to study this reaction experimentally without interference with the other reactions. We do know, however, that the activity of this reaction path is small compared to the path through the oxametallacycle under most reaction conditions [50]. But it is important to include this reaction path in order to explain selectivity trends at low pressures. It is suggested that a vinyl alcohol (CH_2CHOH/O*) is formed (step 12) in the combustion of ethylene [3, and references therein]. Hydrogen is then stripped from the vinyl alcohol and we suggest that the stripping of the first hydrogen (step 13) is the rate-limiting step of this combustion. The combustion of CH_2CHO/O* is therefore assumed to be very fast and it is ignored that step 14 is clearly not elementary.

Expressions for the reaction rates of the elementary reactions in Table 1 are displayed in Table 2. The mass and site balances solved in this work are displayed in Table 3 and Table 4. Note that a forward rate constant (Arrhenius parameters) and equilibrium constant (frequencies and ground state energy) are needed for each elementary reaction. By including a reference pressure ($P^{\ominus} = 100$ kPa) in the rate expressions of the elementary reactions in Table 2 a number of advantages are obtained. First, the equilibrium constants are dimensionless. Secondly, all rate constants and preexponential factors become turnover frequencies (TOF) with the unit molecules per site per second.

In this work we only deal with initial rates; i.e., simulations are compared to steady-state kinetics measured in differential reactors. By a differential reactor it is implied

Table 2
Rate equations for the kinetic model based on reaction steps 1 to 17

$$r_1 = k_1 \frac{P_{O_2}}{P^\ominus}\theta_* - \frac{k_1}{K_1}\theta_{O_2^*}$$
$$r_2 = k_2\theta_{O_2^*}\theta_* - \frac{k_2}{K_2}\theta_{O^*}^2$$
$$r_3 = k_3 \frac{P_{O_2}}{P^\ominus}\theta_{O^*}^2 - \frac{k_3}{K_3}\theta_{O/O^*}^2$$
$$r_4 = k_4 \frac{P_{C_2H_4}}{P^\ominus}\theta_{O^*} - \frac{k_4}{K_4}\theta_{C_2H_4/O^*}$$
$$r_5 = k_5\theta_{C_2H_4/O^*}\theta_{O/O^*} - \frac{k_5}{K_5}\theta_{CH_2CH_2O/O^*}\theta_{O^*}$$
$$r_6 = k_6 \frac{P_{C_2H_4O}}{P^\ominus}\theta_{O^*} - \frac{k_6}{K_6}\theta_{C_2H_4O/O^*}$$
$$r_7 = k_7\theta_{CH_2CH_2O/O^*} - \frac{k_7}{K_7}\theta_{C_2H_4O/O^*}$$
$$r_8 = k_8\theta_{CH_2CH_2O/O^*} - \frac{k_8}{K_8}\theta_{CH_3CHO/O^*}$$
$$r_9 = k_9\theta_{CH_3CHO/O^*} - \frac{k_9}{K_9}\frac{P_{CH_3CHO}}{P^\ominus}\theta_{O^*}$$
$$r_{10} = k_{10}\theta_{CH_3CHO/O^*}\theta_{O^*}^6 - \frac{k_{10}}{K_{10}}\theta_{CO_2^*}^2\theta_{OH^*}^4\theta_*$$
$$r_{11} = k_{11}\frac{P_{C_2H_4}}{P^\ominus}\theta_* - \frac{k_{11}}{K_{11}}\theta_{C_2H_4^*}$$
$$r_{12} = k_{12}\theta_{C_2H_4/O^*}\theta_{O^*} - \frac{k_{12}}{K_{12}}\theta_{CH_2CHOH/O^*}\theta_*$$
$$r_{13} = k_{13}\theta_{CH_2CHOH/O^*}\theta_{O^*} - \frac{k_{13}}{K_{13}}\theta_{CH_2CHO/O^*}\theta_{OH^*}$$
$$r_{14} = k_{14}\theta_{CH_2CHO/O^*}\theta_{O^*}^5 - \frac{k_{14}}{K_{14}}\theta_{CO_2^*}^2\theta_{OH^*}^3\theta_*$$
$$r_{15} = k_{15}\theta_{OH^*}^2 - \frac{k_{15}}{K_{15}}\theta_{H_2O^*}\theta_{O^*}$$
$$r_{16} = k_{16}\theta_{CO_2^*} - \frac{k_{16}}{K_{16}}\frac{P_{CO_2}}{P^\ominus}\theta_*$$
$$r_{17} = k_{17}\theta_{H_2O^*} - \frac{k_{17}}{K_{17}}\frac{P_{H_2O}}{P^\ominus}\theta_*$$

K_i are the equilibrium constants calculated from the molecular partition functions of the intermediates, k_i are the rate constants assumed to be of the Arrhenius form, θ_X is the coverage of species X, and $P^\ominus$ is the thermodynamic reference pressure.

Table 3
Mass balances of gas-phase species for the microkinetic model applied to a steady-state plug flow reactor

$$\frac{dF}{dm} = a\cdot\rho_s\cdot(-r_1 - r_3 - r_4 - r_6 + r_9 - r_{11} + r_{16} + r_{17})$$
$$\frac{dx_{N_2}}{dm} = a\cdot\rho_s\cdot\frac{-x_{N_2}\cdot(-r_1 - r_3 - r_4 - r_6 + r_9 - r_{11} + r_{16} + r_{17})}{F}$$
$$\frac{dx_{O_2}}{dm} = a\cdot\rho_s\cdot\frac{-r_1 - r_3 - x_{O_2}\cdot(-r_1 - r_3 - r_4 - r_6 + r_9 - r_{11} + r_{16} + r_{17})}{F}$$
$$\frac{dx_{C_2H_4}}{dm} = a\cdot\rho_s\cdot\frac{-r_4 - r_{11} - x_{C_2H_4}\cdot(-r_1 - r_3 - r_4 - r_6 + r_9 - r_{11} + r_{16} + r_{17})}{F}$$
$$\frac{dx_{C_2H_4O}}{dm} = a\cdot\rho_s\cdot\frac{-r_6 - x_{C_2H_4O}\cdot(-r_1 - r_3 - r_4 - r_6 + r_9 - r_{11} + r_{16} + r_{17})}{F}$$
$$\frac{dx_{CH_3CHO}}{dm} = a\cdot\rho_s\cdot\frac{r_9 - x_{CH_3CHO}\cdot(-r_1 - r_3 - r_4 - r_6 + r_9 - r_{11} + r_{16} + r_{17})}{F}$$
$$\frac{dx_{CO_2}}{dm} = a\cdot\rho_s\cdot\frac{r_{16} - x_{CO_2}\cdot(-r_1 - r_3 - r_4 - r_6 + r_9 - r_{11} + r_{16} + r_{17})}{F}$$
$$\frac{dx_{H_2O}}{dm} = a\cdot\rho_s\cdot\frac{r_{17} - x_{H_2O}\cdot(-r_1 - r_3 - r_4 - r_6 + r_9 - r_{11} + r_{16} + r_{17})}{F}$$

F [mol/s] is the flow of gas, x_i is mole fractions, m [kg] is the catalyst mass, a is the specific area [m^2/kg], ρ_s [mol/m^2] is the site density, and r_i [s^{-1}] is the rate of the ith elementary step.

Table 4
Steady-state site balances of adsorbates and free sites for the microkinetic model

$$\frac{d\theta_{O_2^*}}{dt} = r_1 - r_2 = 0$$
$$\frac{d\theta_{O^*}}{dt} = 2r_2 - 2r_3 - r_4 + r_5 - r_6 + r_9 - 6r_{10} - r_{12} - r_{13} - 5r_{14} + r_{15} = 0$$
$$\frac{d\theta_{O/O^*}}{dt} = 2r_3 - r_5 = 0$$
$$\frac{d\theta_{C_2H_4/O^*}}{dt} = r_4 - r_5 - r_{12} = 0$$
$$\frac{d\theta_{CH_2CH_2O/O^*}}{dt} = r_5 - r_7 - r_8 = 0$$
$$\frac{d\theta_{C_2H_4O/O^*}}{dt} = r_6 + r_7 = 0$$
$$\frac{d\theta_{CH_3CHO/O^*}}{dt} = r_8 - r_9 - r_{10} = 0$$
$$\frac{d\theta_{C_2H_4^*}}{dt} = r_{11} = 0$$
$$\frac{d\theta_{CH_2CHOH/O^*}}{dt} = r_{12} - r_{13} = 0$$
$$\frac{d\theta_{CH_2CHO/O^*}}{dt} = r_{13} - r_{14} = 0$$
$$\frac{d\theta_{OH^*}}{dt} = 4r_{10} + r_{13} + 3r_{14} - 2r_{15} = 0$$
$$\frac{d\theta_{H_2O^*}}{dt} = r_{15} - r_{17} = 0$$
$$\frac{d\theta_{CO_2^*}}{dt} = 2r_{10} + 2r_{14} - r_{16} = 0$$
$$\theta_* = 1 - \theta_{O_2^*} - \theta_{O^*} - \theta_{O/O^*} - \theta_{C_2H_4/O^*} - \theta_{CH_2CH_2O/O^*} - \theta_{C_2H_4O/O^*} - \theta_{CH_3CHO/O^*} - \theta_{C_2H_4^*} - \theta_{CH_2CHOH/O^*} - \theta_{CH_2CHO/O^*} - \theta_{OH^*} - \theta_{H_2O^*} - \theta_{CO_2^*}$$

θ_i is coverage of intermediates, t [s] is time, r_i [s^{-1}] is the rate of the ith elementary reaction.

that the reaction conditions do not change during a measurement and the rate is constant through space or time of the measurement. Of course differential reactors do not exist in reality; however, if conversions are below ∼5–10% the differential reactor model is usually a good approximation. Using differential reactor data only the initial reactant pressure and temperature are of importance, while flow, site density, number of sites, catalyst mass, reactor configuration, etc. are irrelevant. In this work we do not deal with product inhibition or secondary reactions of formed products, although the microkinetic model could handle such complications.

2.2. Model catalyst

It is assumed that the active phase of the silver catalyst is the Ag(111) facet, because it is the thermodynamically stable facet and therefore suspected to be the most abundant facet on the industrial catalyst. When possible, model parameters have been derived from experiments on Ag(111). However, in some cases the Ag(110) surface has been used due to the absence of appropriate experimental data for Ag(111). Experimental data by Campbell and coworkers [50,51] and Grant and Lambert [42] on Ag(111) and Ag(110) show that the activities of Ag(111) and Ag(110) are very similar. Furthermore, the single crystals exhibit the same kinetic trends as more realistic supported catalysts, indicating that Ag(111) is an excellent model catalyst [50,51,97].

Even though the reaction seems to be structure insensitive comparing Ag(111) and Ag(110), a very puzzling particle-

size effect may be observed [19,97]: Single crystals have a much higher activity than conventional catalysts. The activity is claimed to decrease with decreasing particle size especially in the region 300–500 Å [19]. However, other trends have also been observed [97, and references therein]. The nature of this size effect is not clear. A very simple explanation was offered by Campbell [68] who showed that area measurements of silver catalysts by oxygen chemisorption could be seriously flawed in the presence of chlorine and other impurities. Campbell therefore suggested that the low activities on more realistic catalysts are due to impurities. From kinetics, the size effect seems to only influence the density of sites, while the mechanism remains the same, cf. Section 3. Different site densities are therefore used for different catalysts in the present work, but all other parameters in the model are identical.

On Ag(111) the density of sites (d) is estimated from oxygen chemisorption resulting in a saturation coverage of approximately 0.5 ML in UHV, which combined with the fact that a Ag(111) facet has 1.38×10^{15} surface atoms per square centimeter gives a site density of 6.9×10^{18} sites/m^2. This site density has been used in establishing model parameters from surface science experiments on Ag(111). Note that an active site (*) according to above consists of two Ag surface atoms.

2.3. Model parameters

The equilibrium constants appearing in the microkinetic model are calculated using statistical thermodynamics from parameters for gas-phase molecules and adsorbates. The central parameters are vibrational frequencies and ground state energies. All parameters for gas-phase molecules can be extracted from the NIST database or equivalent [98]. For the adsorbates, vibrational frequencies can be determined from spectroscopic measurements; e.g., EELS, IR, and Raman or from DFT calculations. It is not always possible to establish all the vibrations of intermediates from experiment or calculation. The remaining vibrations are assigned realistic values by guessing or applying simple models. The sensitivity of the model to the values of these guessed parameters has been analyzed and they are not critical regarding the overall predictions of the microkinetic model. Ground state energies can be determined by simulation of TPD experiments and measurements of sticking coefficients. Rate constants are determined from sticking measurements, TPD/TPR experiments, and steady-state kinetics on Ag(111).

How the parameters have been determined will be explained in the following and the results are summarized in Tables 5–8. For more details on the method of parameter estimation we refer to the literature [11] and the analysis of TPD and sticking below. We would like to emphasize that the enthalpy reported in Tables 5–7 for different species is the standard enthalpy of formation at 298.15 K; i.e., the enthalpy needed to form the species from its elements in the standard state. In order to calculate the ground state energy of a species the calculation below should be performed

$$E_g = H_{tot} - (H_{vib} + H_{trans} + H_{rot}), \tag{6}$$

where E_g is the ground state energy, H_{tot} is the total enthalpy as reported in Tables 5–7, and H_{trans}, H_{vib}, and H_{rot} are the translational, vibrational, and rotational enthalpy, respectively, of the species. Furthermore, one should note that for species X adsorbed on a surface oxide site X/O* the enthalpy of O* is included in the tabulated enthalpies for X/O*. Therefore to calculate the enthalpy change for forming an arbitrary intermediate Y such as heat of adsorption one should just use the tabulated enthalpies in combination with the elementary reactions tabulated in Table 1 and Hess's law.

The first-order desorption process in UHV for a generic gas-phase molecule A is given by

$$\frac{d\theta_{A^*}}{dt} = -\frac{k}{K}\theta_{A^*}, \tag{7}$$

where k is the rate constant of adsorption, K is the equilibrium constant, and θ_{A^*} is the coverage of A. The rate constant k is found by equating the initial adsorption rate

Table 5
Model parameters of gas-phase molecules for the statistical thermodynamical treatment

Species	Parameters
O_2	$B = 1.45$, $\sigma = 2$, $\nu_1 = 1580.0$, $H = 0$, $T = 298.15$ K [98]
C_2H_4	$A = 4.83$, $B = 1.00$, $C = 0.83$, $\sigma = 4$, $\nu_1 = 3026.4$, $\nu_2 = 1622.9$, $\nu_3 = 1342.2$, $\nu_4 = 1023.0$, $\nu_5 = 3102.5$, $\nu_6 = 1222.0$, $\nu_7 = 949.3$, $\nu_8 = 943.0$, $\nu_9 = 3105.5$, $\nu_{10} = 826.0$, $\nu_{11} = 2988.7$, $\nu_{12} = 1443.5$, $H = 52.467$ kJ/mol, $T = 298.15$ K [98]
C_2H_4O	$A = 0.854$, $B = 0.736$, $C = 0.47$, $\sigma = 2$, $\nu_1 = 3005.0$, $\nu_2 = 1490.0$, $\nu_3 = 1266.0$, $\nu_4 = 1120.0$, $\nu_5 = 877.0$, $\nu_6 = 3063.0$, $\nu_7 = 1345.0$, $\nu_8 = 807.0$, $\nu_9 = 3019.0$, $\nu_{10} = 1470.0$, $\nu_{11} = 1153.0$, $\nu_{12} = 892.0$, $\nu_{13} = 3079.0$, $\nu_{14} = 1143.0$, $\nu_{15} = 821.0$, $H = -52.635$ kJ/mol, $T = 298.15$ K [98]
CH_3CHO	$A = 1.902$, $B = 0.338$, $C = 0.303$, $\sigma = 1$, $\nu_1 = 3005.0$, $\nu_2 = 2917.0$, $\nu_3 = 2822.0$, $\nu_4 = 1743.0$, $\nu_5 = 1441.0$, $\nu_6 = 1400.0$, $\nu_7 = 1352.0$, $\nu_8 = 1113.0$, $\nu_9 = 919.0$, $\nu_{10} = 509.0$, $\nu_{11} = 2967.0$, $\nu_{12} = 1420.0$, $\nu_{13} = 867.0$, $\nu_{14} = 763.0$, $\nu_{15} = 150.0$, $H = -166.200$ kJ/mol, $T = 298.15$ K [98]
H_2O	$A = 27.887$, $B = 14.511$, $C = 9.280$, $\sigma = 2$, $\nu_1 = 1594.7$, $\nu_2 = 3651.1$, $\nu_3 = 3755.9$, $H = -241.818$ kJ/mol, $T = 298.15$ K [98]
CO_2	$B = 0.39038$, $\sigma = 2$, $\nu_1 = 667.3(2)$, $\nu_2 = 1384.26$, $\nu_3 = 2349.49$, $H = -393.15$ kJ/mol, $T = 298.15$ K [98]

A, B and C are the rotational constants [cm^{-1}], σ is the symmetry number, ν_i are the vibrational frequencies [cm^{-1}], and the degeneracy of a frequency is enclosed in parentheses. H is the standard enthalpy of formation.

Table 6
Model parameters of adsorbates for the statistical thermodynamical treatment

Species	Parameters
O^*	$\nu_1 = 350.0$, $\nu_2 = 508.0(2)$, $H = -63.0$ kJ/mol, $T = 298.15$ K [20]
O_2^*	$\nu_1 = 50(2)$, $\nu_2 = 300(2)$, $\nu_3 = 675$, $\nu_4 = 220$, $H = -44.5$ kJ/mol, $T = 298.15$ K [20]
O/O^*	$\nu_1 = 300(2)$, $\nu_2 = 250$, $\nu_3 = 350$, $\nu_4 = 508(2)$, $H = -103.00$ kJ/mol, $T = 298.15$ K [92]
C_2H_4/O^*	$\nu_1 = 110.0$, $\nu_2 = 1557.0$, $\nu_3 = 3009.0$, $\nu_4 = 1316.0$, $\nu_5 = 1050.0$, $\nu_6 = 963.0$, $\nu_7 = 3090.0$, $\nu_8 = 870.0$, $\nu_9 = 3130.0$, $\nu_{10} = 2980.0$, $\nu_{11} = 1440.0$, $\nu_{12} = 500.0$, $\nu_{13} = 540.0$, $\nu_{14} = 30.0$, $\nu_{15} = 50.0(2)$, $\nu_{16} = 20.0(2)$, $\nu_{17} = 508.0(2)$, $\nu_{18} = 350.0$, $H = -52.338$ kJ/mol, $T = 298.15$ K [33,106,107]
C_2H_4O/O^*	$\nu_1 = 835.0$, $\nu_2 = 1220.0$, $\nu_3 = 1540.0$, $\nu_4 = 3017.0$, $\nu_5 = 915.0$, $\nu_6 = 1148.0$, $\nu_7 = 1440.0$, $\nu_8 = 3010.0$, $\nu_9 = 2890.0$, $\nu_{10} = 2820.0$, $\nu_{11} = 2970.0$, $\nu_{12} = 2920.0$, $\nu_{13} = 1080.0$, $\nu_{14} = 1035.0$, $\nu_{15} = 100.0$, $\nu_{16} = 50.0(3)$, $\nu_{17} = 30.0(3)$, $\nu_{18} = 508.0(2)$, $\nu_{19} = 350.0$, $H = -158.00$ kJ/mol, $T = 298.15$ K [33,36,89]
CH_2CH_2O/O^*	$\nu_1 = 344.0$, $\nu_2 = 405.0$, $\nu_3 = 455.0$, $\nu_4 = 717.0$, $\nu_5 = 793.0$, $\nu_6 = 905.0$, $\nu_7 = 996.0$, $\nu_8 = 1052.0$, $\nu_9 = 1218.0$, $\nu_{10} = 1273.0$, $\nu_{11} = 1353.0$, $\nu_{12} = 1446.0(2)$, $\nu_{13} = 2922.0(2)$, $\nu_{14} = 434.0$, $\nu_{15} = 80.0(2)$, $\nu_{16} = 30.0$, $\nu_{17} = 40.0$, $\nu_{18} = 17.0$, $\nu_{19} = 350$, $\nu_{20} = 508.0(2)$, $H = -163.00$ kJ/mol, $T = 298.15$ K [40,42]
CH_3CHO/O^*	$\nu_1 = 3005.0$, $\nu_2 = 3064.0$, $\nu_3 = 1155.0$, $\nu_4 = 1490.0$, $\nu_5 = 1345.0$, $\nu_6 = 892.0$, $\nu_7 = 1266.0$, $\nu_8 = 807.0$, $\nu_9 = 3080.0$, $\nu_{10} = 1120.0$, $\nu_{11} = 3020.0$, $\nu_{12} = 1143$, $\nu_{13} = 70.0$, $\nu_{14} = 877.0$, $\nu_{15} = 1470.0$, $\nu_{16} = 50.0(2)$, $\nu_{17} = 20.0(4)$, $\nu_{18} = 350$, $\nu_{19} = 508.0(2)$, $H = -269.700$ kJ/mol, $T = 298.15$ K [37]

ν_i are the vibrational frequencies [cm^{-1}] and the degeneracy of a frequency is enclosed in parentheses. H is the standard enthalpy of formation.

Table 7
Model parameters of adsorbates for the statistical thermodynamical treatment

Species	Parameters
$C_2H_4^*$	$\nu_1 = 110.0$, $\nu_2 = 1557.0$, $\nu_3 = 3009.0$, $\nu_4 = 1316.0$, $\nu_5 = 1050.0$, $\nu_6 = 963.0$, $\nu_7 = 3090.0$, $\nu_8 = 870.0$, $\nu_9 = 3130.0$, $\nu_{10} = 2980.0$, $\nu_{11} = 1440.0$, $\nu_{12} = 500.0$, $\nu_{13} = 540.0$, $\nu_{14} = 30.0$, $\nu_{15} = 50.0(2)$, $\nu_{16} = 20.0(2)$, $H = 17.70$ kJ/mol, $T = 298.15$ K [33,106,107]
CH_2CHOH/O^*	$\nu_1 = 1885.0$, $\nu_2 = 1220.0$, $\nu_3 = 1540.0$, $\nu_4 = 3017.0$, $\nu_5 = 1915.0$, $\nu_6 = 1148.0$, $\nu_7 = 1440.0$, $\nu_8 = 3010.0$, $\nu_9 = 2890.0$, $\nu_{10} = 1820.0$, $\nu_{11} = 2970.0$, $\nu_{12} = 2920.0$, $\nu_{13} = 3080.0$, $\nu_{14} = 1035.0$, $\nu_{15} = 100.0(2)$, $\nu_{16} = 1000.0$, $\nu_{17} = 30.0(2)$, $\nu_{18} = 500.0$, $\nu_{19} = 300.0$, $\nu_{20} = 100.0(2)$, $\nu_{21} = 350.0$, $H = -120.00$ kJ/mol, $T = 298.15$ K
CH_2CHO/O^*	$\nu_1 = 110.0$, $\nu_2 = 1557.0$, $\nu_3 = 3010.0$, $\nu_4 = 1316.0$, $\nu_5 = 1050.0$, $\nu_6 = 963.0$, $\nu_7 = 3090.0$, $\nu_8 = 870.0$, $\nu_9 = 3130.0$, $\nu_{10} = 2980.0$, $\nu_{11} = 1440.0$, $\nu_{12} = 500.0$, $\nu_{13} = 540.0$, $\nu_{14} = 30.0$, $\nu_{15} = 50.0(2)$, $\nu_{16} = 20.0(2)$, $\nu_{17} = 508.0(2)$, $\nu_{18} = 350.0$, $\nu_{19} = 350.0$, $\nu_{20} = 20.0(2)$, $\nu_{21} = 508(2).0$, $H = -58.00$ kJ/mol, $T = 298.15$ K
H_2O^*	$\nu_1 = 27.9$, $\nu_2 = 27.9(2)$, $\nu_3 = 740(3)$, $\nu_4 = 1660$, $\nu_5 = 3410(2)$, $H = -289.5$ kJ/mol, $T = 298.15$ K [38]
OH^*	$\nu_1 = 280.0$, $\nu_2 = 49.3(2)$, $\nu_3 = 670.0(2)$, $\nu_4 = 3380.0$, $H = -185.00$ kJ/mol, $T = 298.15$ K [38]
CO_2^*	$\nu_1 = 410$, $\nu_2 = 30.6(2)$, $\nu_3 = 12.71$, $\nu_4 = 667(2)$, $\nu_5 = 1365$, $\nu_6 = 2350$, $H = -433.0$ kJ/mol, $T = 298.15$ K [39]

ν_i are the vibrational frequencies [cm^{-1}] and the degeneracy of a frequency is enclosed in parentheses. H is the standard enthalpy of formation.

Table 8
Forward and backward Arrhenius parameters for elementary reactions in the microkinetic model at 500 K

Step i	A_i [s^{-1}]	$H_i^{\ddagger}$ [kJ/mol]	A_{-i} [s^{-1}]	$H_{-i}^{\ddagger}$ [kJ/mol]	Ref.
1	2.71×10^5	5.7	1.1×10^{12}	47.3	[20]
2	4.0×10^{12}	75.0	8.0×10^{14}	157.5	[20]
3	2.0×10^7	20.0	1.3×10^{15}	96.9	[11,95]
4	7.2×10^7	0.0	2.2×10^{11}	37.1	[33]
5	9.0×10^{14}	112.0	5.3×10^{14}	183.3	[51]
6	1.95×10^8	0.0	4.8×10^{12}	39.1	[34–36]
7	1.13×10^{13}	95.0	2.11×10^{12}	93.5	[4,51,52]
8	9.0×10^{12}	95.0	4.5×10^{10}	204.3	[4,51,52]
9	2.9×10^{13}	41.9	2.6×10^9	4.4	[37]
10	2.0×10^{20}	11.0	5.3×10^{13}	791.6	
11	7.2×10^7	0.0	2.2×10^{11}	30.1	[33]
12	4.0×10^{11}	32.0	3.1×10^{14}	42.8	
13	2.6×10^{13}	86.0	1.3×10^9	106.1	
14	1.0×10^{20}	0.0	5.5×10^{13}	906.6	
15	1.4×10^{10}	65.6	1.0×10^{11}	50.0	[38]
16	3.6×10^{14}	38.9	1.0×10^8	0.0	[39]
17	5.9×10^{14}	46.6	1.4×10^9	0.0	[38]

A is the prefactor and $H^{\ddagger}$ is the activation enthalpy.

with the initial sticking rate

$$k = \frac{\sigma_0 P^{\ominus}}{d\sqrt{2\pi m k_B T}}, \tag{8}$$

where σ_0 is the initial sticking coefficient, $P^{\ominus}$ is the thermodynamic reference pressure, m is the mass of A, k_B is Boltzmann's constant, and T is the temperature. Substituting Eq. (8) into Eq. (7) the following equation is obtained:

$$\frac{d\theta_{A^*}}{dt} = -\frac{\sigma_0 P^{\ominus}}{d\sqrt{2\pi m k_B T} K}\theta_{A^*}. \tag{9}$$

Experimental TPD spectra can be simulated by integrating Eq. (9) with numerical techniques. The ground state energy comes into play through the equilibrium constant and is optimized until the experimental peak temperature is reproduced.

The sticking probability of ethylene, ethylene oxide, water, carbon dioxide, and acetaldehyde is close to unity [33,36–39], and it is reasonable to assume an adsorption activation barrier of zero for these species. From this assumption and the measured sticking probabilities rate

constants of steps 4, 6, 9, 11, 16, 17 are determined. The TPD peak temperature of adsorbed ethylene, ethylene oxide, and acetaldehyde increases with oxygen coverage [33,35–37,50,66]. The ground state energy of $C_2H_4^*$ has been determined from a peak temperature of 148 K, C_2H_4/O^* from 175 K, C_2H_4O/O^* from 175 K, H_2O^* from 170 K, CO_2^* from 145 K, and CH_3CHO/O^* from 160 K. The heat of adsorption and the simulated TPD peak temperatures of these species are similar to the reported values in the literature [31–33,35–39,50,66]. The Arrhenius parameters for step 15 and the stability of OH* are determined in such a way that the experimental formation of OH* at ∼250 K and the recombination of OH* at ∼320 K are reproduced [38].

The rate constants of steps 1–2 and the ground state energies of O_2^* and O* are established from simulation of sticking probability measurements and TPD experiments [84]. It should be emphasized that the model predicts the low dissociative sticking probability of 10^{-6} at 500 K as observed experimentally [20]. Furthermore, the heat of adsorption of O* (126 kJ/mol O_2) is close to the reported experimental values in the literature (∼100–∼170 kJ/mol O_2) [20,92,99].

The preexponential of step 3 has been estimated from transition state theory [11] and the activation barrier has been obtained from measurements of adsorption activation energies [95]. The ground state energy of electrophilic oxygen has been established by fitting to steady-state kinetics on Ag(111) measured by Campbell [51], cf. Figs. 1–3. The necessary heat of adsorption of O/O* in order to explain the kinetics turns out to be ∼80 kJ/mol O_2 almost identical to the heat of adsorption measured above 0.5 ML on silver (∼75 kJ/mol O_2) [92].

The stability of the oxametallacycle is found from TPR experiments [42,46,100]. Exposing silver predosed with surface and subsurface oxygen to large ethylene doses at 300 K results in desorption of ethylene oxide and acetaldehyde in a common peak (360–420 K) in a subsequent TPD experiment [42,46,100]. Originally it was believed that adsorbed ethylene and atomic oxygen reacted to form ethylene oxide at 360–420 K. However, ethylene is not stable above 200 K in UHV [32,33,50,66]. A more consistent interpretation of this experiment is that a stable oxametallacycle is formed during the ethylene exposure at 300 K, which desorbs/react at 360–420 K. This is also consistent with the work of Tysoe et al. [31]. Furthermore, Grant and Lambert discovered that ethylene oxide could adsorb at 300 K by using high ethylene oxide doses [52]. However, ethylene oxide desorbs below 200 K in UHV [32,33,35,36]. Again this suggests that the authors produced an oxametallacycle instead of adsorbed ethylene oxide as suggested in the original work. Grant and Lambert measured the sticking probability of this process to 2.3×10^{-8} at 300 K [52]. Using these experiments the stability of the oxametallacycle is estimated [84]. Alternatively, the experiments of Linic and Barteau [70] could have been used. Here the oxametallacycle was produced from ethylene oxide on Ag(111) at 250 K. The oxametallacycle reforms to produce ethylene oxide at ∼300 K. The parameters will not vary significantly whether one or the other experiment is chosen. There are two reasons that the experiments of Grant and Lambert [42] were chosen to extract parameters instead of the apparently more direct experiments of Linic and Barteau. First of all, in the TPR experiments of Grant and Lambert, the oxametallacycle is formed from reaction between ethylene and oxygen and is therefore the interesting oxametallacycle in ethylene epoxidation. It is known that a number of similar oxametallacycles may exist [71, and references therein]. Secondly, this leads to reinterpretation that offers a consistent explanation for a number of important TPR experiments in the literature [42,46,100]. Finally, the exact values are not critical to the conclusions drawn in this work. Interestingly, Linic and Barteau estimated the activation energy of ring closure to ∼70 kJ/mol using a Redhead analysis, which is close to the value predicted in the microkinetic model (95 kJ/mol). In addition, Mavrikakis et al. [101] calculated a stability of ∼42 kJ/mol for the oxametallacycle compared to gas-phase ethylene oxide, which is close to the value predicted by the microkinetic model (47.4 kJ/mol).

The Arrhenius parameters of step 5 have been determined by fitting the Arrhenius plot measured by Campbell [51] on Ag(111), cf. Fig. 1. The rate constants of steps 7 and 8 have been established by fitting selectivity on Ag(111), the sticking probability of oxametallacycle, and the combustion of ethylene oxide, cf. Fig. 7. The rate of step 10 is known to be very fast which is ensured by the selected Arrhenius parameters [6,7,57].

The suggested mechanism for combustion of ethylene by nucleophilic oxygen through a vinyl alcohol intermediate is very speculative and a number of other intermediates such as formate, acetate, or glycol could be important. Needless to say, it has not been possible to deduce the parameters for this combustion explicitly. Instead realistic values have been chosen which reproduce the experimental effects.

The estimated preexponentials depicted in Table 8 all attain physically realistic values except steps 10 and 14, which are not elementary. Transition state theory (TST) predicts a prefactor of about 10^{13} s^{-1} for first-order surface reactions varying a few orders of magnitude dependent of the nature of the transition state (mobile/immobile) [11]. Experimentally, preexponentials vary from 10^{10} to 10^{16} s^{-1} for surface reactions and desorption [102]. The high preexponential of O* desorption (Table 8) is similar to values reported in the literature [20, and references therein]. The preexponential of step 5 is high which is also reflected by the high turnover frequencies measured on single crystals [51], cf. Figs. 1–3.

3. Results

In this section the model (Tables 1–4) has been applied to a differential reactor and turnover frequencies and selectivity (S) have been calculated under various reaction conditions.

The selectivity is defined as

$$S = \frac{-r_6}{-r_6 + \frac{1}{2}r_{16}}. \quad (10)$$

The coverage of surface oxide sites (θ_{oxide}) consists of the coverage of O* sites plus the /O* sites covered by other intermediates; i.e., the oxide coverage is defined by

$$\theta_{\text{oxide}} = \theta_{\text{O}^*} + \theta_{\text{O/O}^*} + \theta_{\text{C}_2\text{H}_4/\text{O}^*} + \theta_{\text{CH}_2\text{CH}_2\text{O/O}^*} + \theta_{\text{C}_2\text{H}_4\text{O/O}^*} + \theta_{\text{CH}_3\text{CHO/O}^*} + \theta_{\text{CH}_2\text{CHOH/O}^*} + \theta_{\text{CH}_2\text{CHO/O}^*}. \quad (11)$$

The coverage of surface oxide (θ_{oxide}) is a measure of the active sites present for epoxidation. The coverage of O* corresponds to the unoccupied sites for epoxidation. Alternatively, one could look at θ_{oxide} as a site balance for $Ag^{\delta+}$ sites assuming that each O* results in one $Ag^{\delta+}$ site.

In Figs. 1–3 the model is used to simulate the single crystal experiments of Campbell [51] and Grant and Lambert [42]. Recall that the experiments of Campbell were used to establish the Arrhenius parameters of step 5 and the ground state energy of O/O*.

In Fig. 1 the model is used to simulate Arrhenius plots. The model reproduces the data of Campbell very closely. In particular, the model successfully captures the curved trend in the Arrhenius plot, i.e., a high activation energy at low temperatures and a low activation energy at high temperatures. The model seems generally to reproduce the activation energy as measured by Grant and Lambert, but the predicted activities are on the low side. It appears that the model generally underpredicts activities at low oxygen pressures (below $\sim$10 kPa). However, the model captures the experimental trends and it is quantitatively accurate within a factor of 2–3 even at low pressures, which is satisfying in view of the number of other observations reproduced by the model. It should be noted that both simulation and experiment predict a curved Arrhenius plot in the experiments of Campbell but a more or less straight Arrhenius plot in the case of Grant and Lambert. The reason for this different behavior is that Campbell used moderate reactant pressures while Grant and Lambert used very low pressures (see Fig. 1). As will be discussed in Section 4.4 the apparent activation energy depends on the chosen reaction conditions.

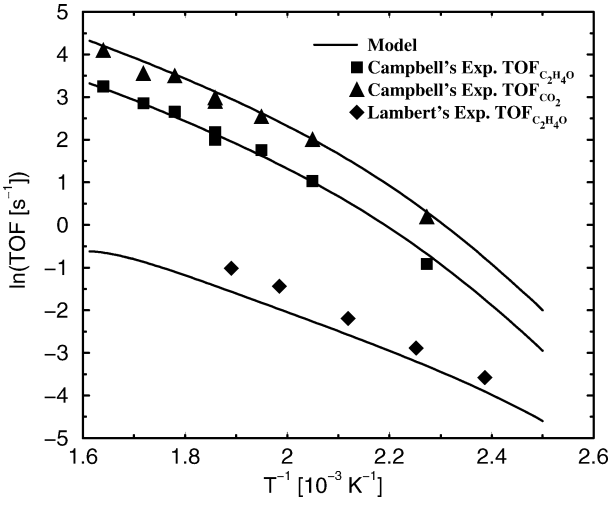

Fig. 1. Simulated and experimental Arrhenius plot of C_2H_4O and CO_2 formation on Ag(111). Campbell's experiments [51] were done at $P_{O_2} = 20$ kPa and $P_{C_2H_4} = 2.66$ kPa while the experiment of Grant and Lambert [42] was done at $P_{O_2} = 0.67$ kPa and $P_{C_2H_4} = 0.67$ kPa.

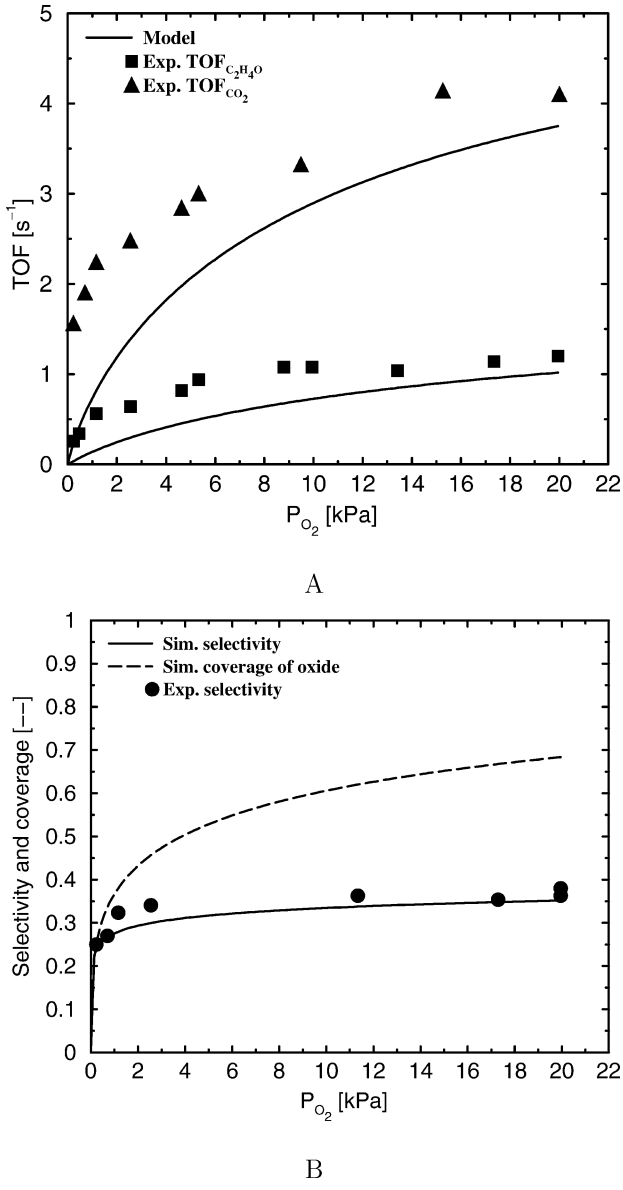

Fig. 2. Simulated and experimental turnover frequencies of C_2H_4O and CO_2 formation (A) and selectivity and oxide coverage (B) versus oxygen pressure on Ag(111). $T = 490$ K and $P_{C_2H_4} = 0.55$ kPa. Experimental data are extracted from [51].

The model also reproduces the production of CO_2 very well and therefore the selectivity. It is indirectly observed from Fig. 1 that the selectivity remains almost constant with temperature. Furthermore, the activation energies of both epoxidation and combustion are almost identical. These features would be very hard to explain without introducing a

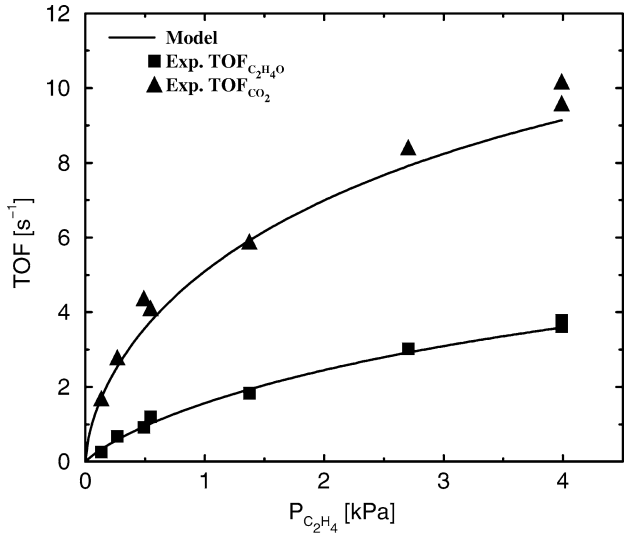

A

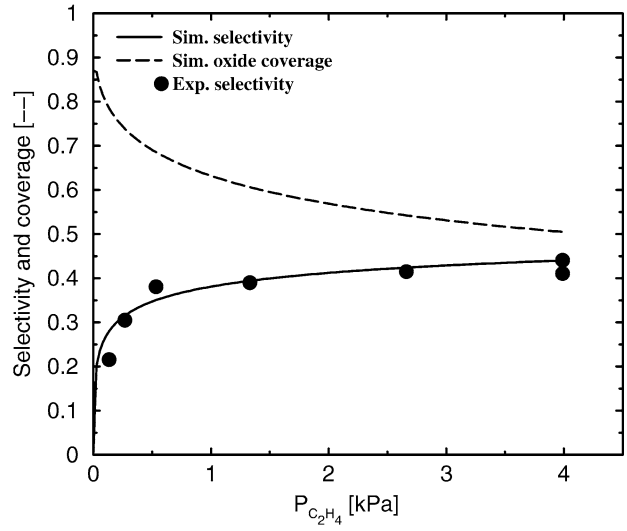

B

Fig. 3. Simulated and experimental turnover frequencies of C_2H_4O and CO_2 formation (A) and selectivity and oxide coverage (B) versus ethylene pressure on Ag(111). $T = 490$ K and $P_{O_2} = 20$ kPa. Experimental data are extracted from [51].

common slow reaction step for epoxidation and combustion as pointed out in the work of Campbell [50,51,68].

Fig. 2 shows experimental and simulated activities, selectivities, and O* coverage versus oxygen pressure on Ag(111). The model captures the activity trends for both epoxidation and combustion. However, again it is apparent that the model underpredicts activities at low oxygen pressures. The model explains the experimental selectivity very well. The selectivity increases with oxygen pressure because the formation of oxametallacycle increases more rapidly with oxygen pressure than the parallel combustion of ethylene through the vinyl alcohol intermediate.

Campbell and co-workers [50,51] measured the coverage of O* under steady-state reaction conditions by transferring the single crystal from a high-pressure cell to UHV. Only O* was thermally stable enough to survive the transfer at 490 K. We propose that the measured O* coverage by Campbell and co-workers corresponds to the coverage of surface oxide defined in the beginning of this section. Because in the transfer to UHV all the intermediates adsorbed on the surface oxide (X/O*) desorbs leaving O* on the surface.

As observed in Fig. 2 the simulated coverage of surface oxide increases with oxygen pressure and levels out below the equilibrium coverage. Similar trends were observed experimentally by Campbell and co-workers [50,51]. Quantitatively, the measured coverage was lower than the simulated. However, Tan et al. [103] pointed out that some of the oxide is lost during transfer due to background reactions with H_2 and CO.

Fig. 3 shows experimental and simulated activities, selectivities, and surface oxide coverage versus ethylene pressure on Ag(111). The model reproduces the activities and selectivity, quantitatively. The simulated surface oxide coverage again qualitatively resembles the measured oxygen coverage by Campbell and co-workers [50,51]. It should be stressed that the quantitative disagreement between measured and calculated oxide coverages is not believed to be a flaw in the model, but due to the experimental difficulties in transferring the oxide from a high-pressure cell to UHV without losing oxygen.

In Fig. 4 the model output is compared to experimental initial rates obtained in different laboratories using different unpromoted catalysts ranging from single crystals to supported catalysts. The oxygen and ethylene pressure and temperature were varied extensively in the reported experiments [4,42,51,53–56,64,104]. Only the site density of each

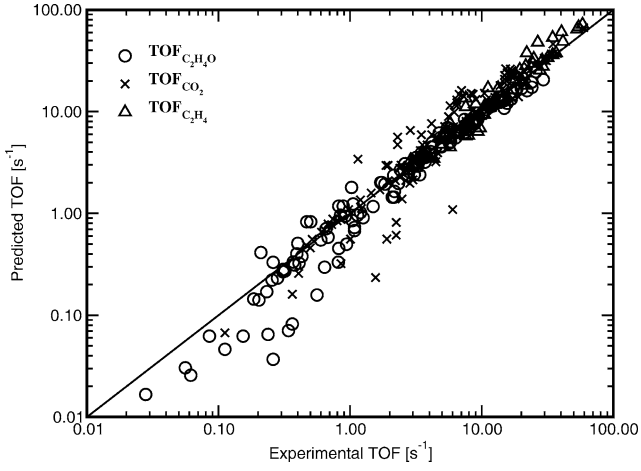

Fig. 4. Predicted versus experimental turnover frequencies of C_2H_4O and CO_2 formation and C_2H_4 consumption. The experimental results are extracted from reported initial rates [4,42,51,53–56,64,104] measured in different laboratories using different unpromoted catalysts ranging from single crystals to realistic supported catalysts. $T = 400$–620 K, $P_{O_2} = 0.13$–1300 kPa, and $P_{C_2H_4} = 0.13$–140 kPa.

catalyst has been fitted in order to establish turnover frequencies corresponding to Ag(111) single crystals while all other parameters are extracted earlier (Section 2.3) from surface science and the single-crystal kinetics of Campbell [51]. It is apparent from Fig. 4 that the model reproduces the experiments surprisingly well. Again only the low activity measurements done at low pressures deviate from the experiments. This demonstrates that the microkinetic model contains the essential chemistry and physics to explain ethylene epoxidation and combustion on silver. Furthermore, this shows that the mechanisms on different unpromoted silver catalysts are identical and the particle-size effect only seems to influence the site density. This model can therefore be used to extract site densities in order to study the particle-size effect. Surprisingly, it has been reported in the literature that the kinetics varies between different laboratories supposedly due to impurities and different reactor configurations [65, and references therein]. This work clearly shows that initial rates can be explained with one consistent model. Since the experimental initial rates are obtained from different datasets in the literature and a site density has been fitted for each catalyst used in the datasets, Fig. 4 may appear less impressive. However, of the $\sim$350 data points besides single-crystal data in Fig. 4 only eight site densities have been fitted. None of the parity plots for individual datasets (not shown) display significant deviations.

In Figs. 5 and 6 the measured epoxidation activities of Harriott and co-workers [53,54] are simulated. These data represent to the best of our knowledge the most extensive data set of initial rates in oxygen and ethylene pressure. Similar experimental and simulated results (not shown) are obtained for combustion activities. Fig. 5 shows the turnover frequency of ethylene oxide formation versus ethylene pressure at different oxygen pressures. The model clearly captures the experimental trends. At low ethylene pressure the turnover frequency increases with ethylene pressure but at higher ethylene pressure the reaction order in ethylene starts to decrease and eventually becomes negative. This results in a maxima in turnover frequencies. The maxima shift to higher ethylene pressure with higher oxygen pressure. Fig. 6 shows the turnover frequency versus oxygen pressure at two different ethylene pressures. The reaction order in oxygen is positive at low oxygen pressures, but starts to decrease and become negative at high oxygen pressures, resulting in a maxima in turnover frequencies. Note that very high pressures are needed to obtain maxima in turnover frequency versus oxygen pressure. As will become apparent later this is due to the fact that the uptake of oxygen is partly rate limiting.

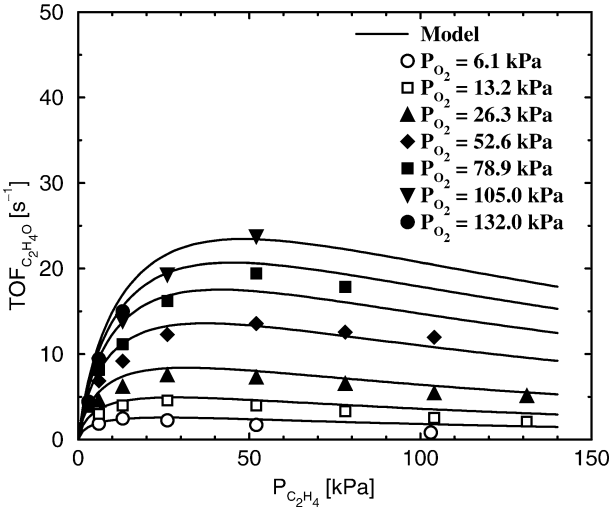

Fig. 5. Simulated and experimental effect of ethylene pressure on the turnover frequency of C_2H_4O formation on an unpromoted α-Al_2O_3-supported Ag catalyst for various oxygen pressures at 493 K. Experimental data are extracted from [53].

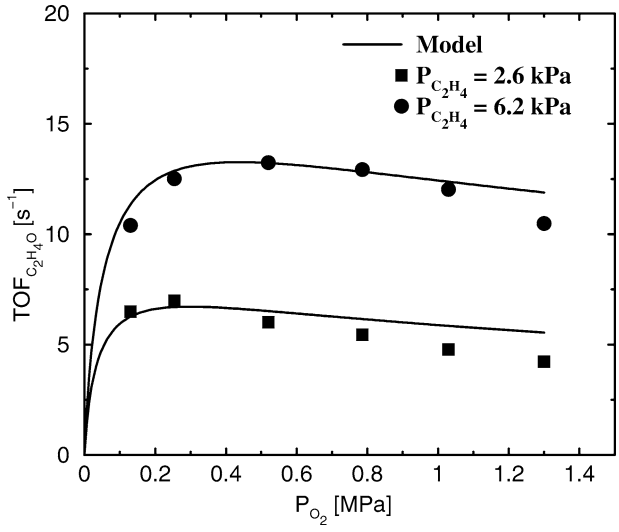

Fig. 6. Simulated and experimental effect of oxygen pressure on the turnover frequency of C_2H_4O formation on an unpromoted α-Al_2O_3-supported Ag catalyst for various ethylene pressures at 493 K. Experimental data are extracted from [54].

We noted earlier that our reaction mechanism does not need a separate combustion route for ethylene oxide. Fig. 7 shows the experimental turnover frequencies of ethylene oxide combustion measured by Dettwiler et al. [4] and model simulation. The model clearly captures the first-order dependence in ethylene oxide pressure and the temperature dependence of ethylene oxide combustion [4,5,57]. Petrov et al. found that the combustion of ethylene oxide starts at 463 K [5], which is similar to the prediction of the model.

4. Discussion

It has been demonstrated above that a microkinetic model consistent with surface science experiments is able to explain a broad range of steady-state kinetic experiments. We would like to emphasize that besides the steady-state kinet-

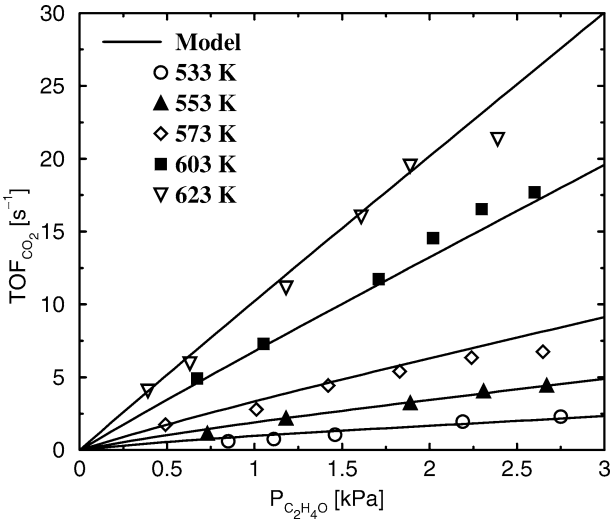

Fig. 7. Rate of ethylene oxide oxidation as a function of ethylene oxide pressure and temperature. $P_{O_2} = 20$ kPa. Experimental data are extracted from [4].

ics presented in the present work the model also explains sticking, TPD, and TPR experiments of the intermediates in the model. In particular, it has been shown by the model that the role of subsurface oxygen could simply be to serve as an oxygen reservoir in the absence of gas-phase oxygen. The model therefore explains a broad range of transient surface science experiments as well. Most of the parameters have been explicitly determined from such transient surface science experiments and only a few of the many parameters in the model have been fitted to steady-state kinetics. The most important of these is the Arrhenius parameters of the surface reaction between adsorbed ethylene and electrophilic oxygen (step 5), which have been fitted to steady-state kinetics on Ag(111). Furthermore, the branching ratio of steps 7 and 8 has been determined from the steady-state selectivity on Ag(111). Few other parameters have been fitted with constraints from surface science experiments to the steady-state combustion of ethylene oxide on supported silver. However, these parameters are only important to the combustion of ethylene oxide and are not critical to the main conclusions of the present work. To the best of our knowledge this is the first time a consistent model describing both the adsorption behavior of oxygen and ethylene and the kinetics of epoxidation, ethylene combustion, and ethylene oxide combustion has been presented. Earlier models only explain the data sets used to deduce them and cannot be extrapolated to significantly different reaction conditions. The rate laws reported in the literature are therefore only appropriate for describing either ethylene-rich or oxygen-rich reaction conditions. As with all mechanistically correct microkinetic models, this is a rather complicated model and so, at first, it is difficult to grasp within this model the importance of the various aspects of the model.

In this section the model will be thoroughly analyzed and the important aspects in ethylene epoxidation are established.

4.1. Degree of rate control

The rate-controlling elementary reactions are identified by using the degree of rate control ($X_{\mathrm{RC},i}$) [105],

$$X_{\mathrm{RC},i} = \frac{\mathrm{d}\ln(R)}{\mathrm{d}\ln(k_i)}, \quad K_i = \text{const}, \tag{12}$$

where R is an overall rate and k_i and K_i are the forward rate constant and equilibrium constant of the ith elementary reaction, respectively. The larger numeric value of $X_{\mathrm{RC},i}$ the greater importance of step r (both forward and backward reaction) on the rate control of R. A negative value of $X_{\mathrm{RC},i}$ indicates that step r inhibits the net rate. Eq. (12) can also be modified to determine selectivity control as will be shown in Section 4.5.

The degree of rate control of the 17 elementary reactions in Table 1 for ethylene oxide formation, CO_2 formation, ethylene consumption, and selectivity has been determined for a wide range of temperature and oxygen and ethylene pressures in a differential reactor. Only 5 elementary reactions of the 17 contained in the model are of importance in the rate and selectivity control, i.e., r_2, r_5, r_7, r_8, and r_{13}. Fig. 8 is an example of calculated degrees of rate control of ethylene oxide formation at partial pressures of oxygen and ethylene and temperatures in the same region as used in the industrial process. The uptake of O* (r_2) and the reaction between electrophilic oxygen (O/O*) and adsorbed ethylene to form an oxametallacycle (r_5) are the most important elementary steps concerning the overall activity. The branching of the oxametallacycle into ethylene oxide (r_7) and acetaldehyde (r_8) are the most important steps in selectivity control. Similar conclusions were reached by Linic and Barteau applying a much simpler microkinetic model and

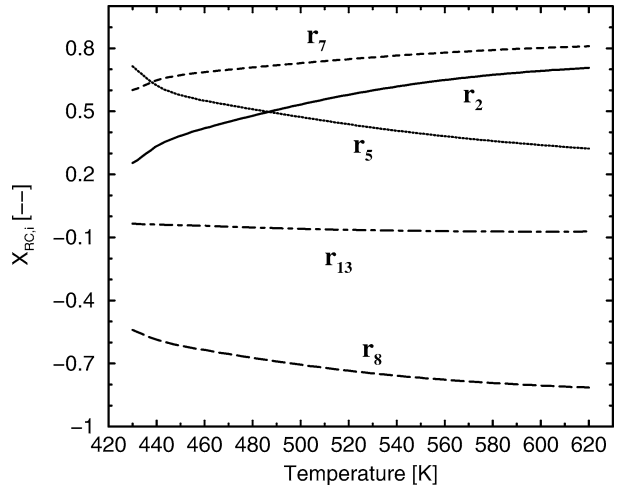

Fig. 8. Degree of rate control for ethylene oxide formation versus temperature at industrial reaction conditions. $P_{O_2} = P_{C_2H_4} = 100$ kPa.

DFT calculations [69,71]. r_7 and r_8 also play a role in overall activity control due to the fact that combustion of acetaldehyde consumes O* while the formation of ethylene oxide does not consume O*. Note in Fig. 8 that $X_{RC,i}$ of r_7 and r_8 is symmetric with opposite signs, which is general. This can be explained by the symmetric branching of the oxametallacycle. The parallel combustion of ethylene by O* through a vinyl alcohol intermediate (r_{13}) has some influence on the overall activity and selectivity at low reactant pressures but are unimportant at industrial conditions, cf. Fig. 8. The relative importance of r_2 and r_5, respectively, depends strongly on reaction conditions. At high O_2:C_2H_4 ratio r_5 is most important but at moderate to low O_2:C_2H_4 ratio r_2 becomes more important. The importance of r_2 also increases with temperature as illustrated in Fig. 8. From Fig. 8 it is apparent that r_2 is the most important activity reaction rate under industrial conditions. It is interesting to note that Harriott and co-workers [53,54] concluded from the experiments in Fig. 5 that the adsorption of oxygen was not rate limiting. The present model which reproduce Harriott and co-workers experiments shows, however, that the adsorption of oxygen is one of the rate-controlling steps under the experimental conditions.

The fact that the adsorption of O* (step 2) is rate limiting has very serious consequences for the model. Due to the fact that O* participates in many different elementary reactions it is not possible to obtain an analytical solution for the model; i.e., the quasi-equilibrium approximation cannot be solved. This complicates the analysis of the model and it is difficult or maybe even impossible to deduce a general analytical rate law for ethylene oxidation. This explains the many different forms of analytical rate expressions and their limited usefulness reported in the literature, but emphasizes the importance of the degree of rate control.

4.2. Coverages

In Fig. 9 the coverage of intermediates is depicted for a differential reactor versus temperature. The pressures of products are therefore very low. Under industrial conditions a significant amount of reaction products is present which leads to a different distribution of coverages than depicted in Fig. 9. However, in the present work only initial rates have been dealt with. In future work product inhibition, reactor profiles, and integral reactor data will be treated. The intermediates not shown in Fig. 9 all have a very short life time and do not occupy a significant amount of sites under these initial reaction conditions. θ_{O^*} is the oxide coverage defined in Section 3. The surface oxide coverage, i.e., the active sites, in epoxidation decreases with temperature, while the coverage of metallic silver sites increases. Significant amounts of electrophilic oxygen (O/O*) and adsorbed ethylene on oxide (C_2H_4/O*) are present in the studied temperature interval. Ethylene adsorbed on metallic silver ($C_2H_4^*$) is also present on the surface, which is in contrast to the suggestion that ethylene cannot adsorb on reduced silver. The reason for this

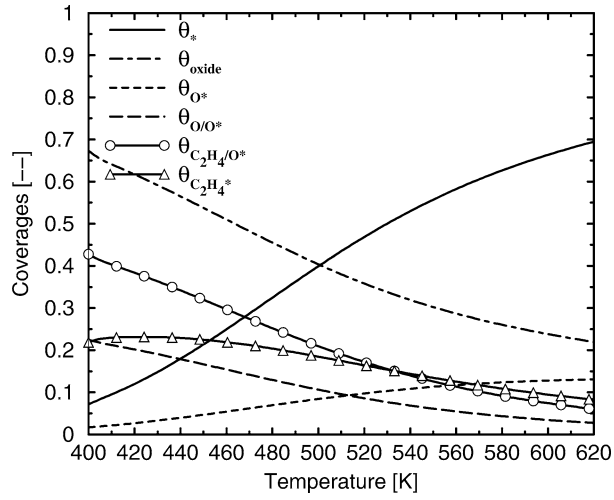

Fig. 9. Calculated coverages of selected intermediates as a function of temperature. $P_{O_2} = P_{C_2H_4} = 100$ kPa.

discrepancy is the high ethylene pressure used in the current simulation compared to the low pressures often used in surface science experiments. The idea that adsorbates with low heats of adsorption ($\sim$40 kJ/mol) cannot be present on catalysts at elevated temperatures is of course wrong. The low heat of ethylene adsorption has even lead to the false conclusion that ethylene epoxidation is an Eley–Rideal mechanism. Unless the adsorption is kinetically controlled an equilibrium coverage dependent on reactant pressure and temperature will be present. Actually, ethylene is the most abundant intermediate. The coverage of adsorbed ethylene on the surface oxide layer is higher than the ethylene coverage on metallic silver even at low surface oxide coverage. Note that the coverage of O* increases with temperature while the coverage of surface oxide (θ_{oxide}) decreases. This can be explained by desorption of X/O* species which leaves O* and only part of the formed O* desorbs. The simulated coverages are believed to be in qualitative agreement with surface science results.

4.3. Reaction orders

Reaction orders (α_i) may be defined as [12]

$$\alpha_i = \frac{\mathrm{d}\ln(R)}{\mathrm{d}\ln(P_i/P^{\ominus})}, \tag{13}$$

where P_i is the pressure of gas i, R is an overall rate, and $P^{\ominus}$ is the reference pressure.

From the Introduction and Figs. 2–6 it is apparent that the reaction orders in oxygen and ethylene vary dramatically with reaction conditions according both to experiments and to the model. This is due to the variation in coverage of intermediates and changes in the degree of rate control of r_2 and r_5, respectively, with reaction conditions.

The reaction orders in both ethylene and oxygen increases with temperature (Fig. 10). The reaction orders in oxygen vary from 1.5 to -0.5 when the oxygen is varied from very

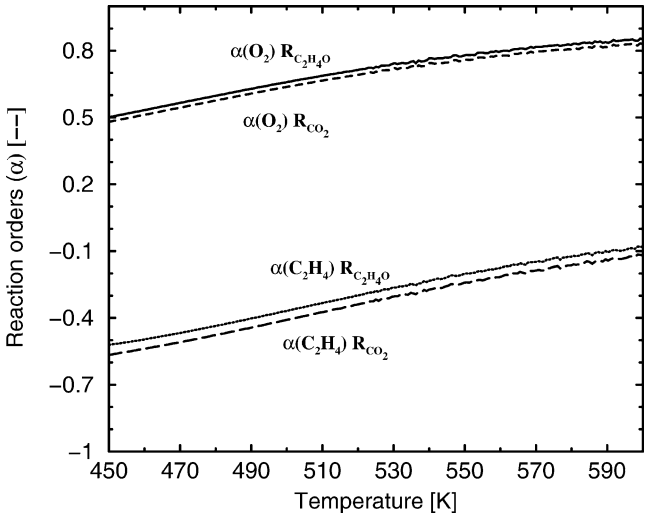

Fig. 10. Calculated reaction orders in oxygen and ethylene pressure as a function of temperature. $P_{O_2} = P_{C_2H_4} = 100$ kPa.

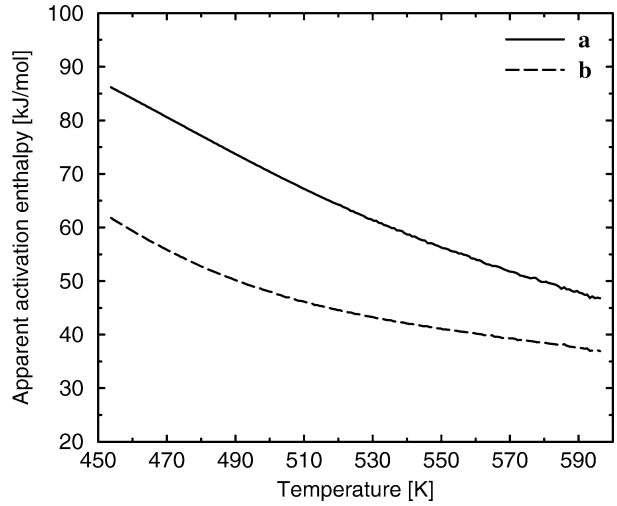

Fig. 11. Simulated apparent activation enthalpy of ethylene oxide formation versus temperature. (a) $P_{O_2} = P_{C_2H_4} = 100$ kPa. (b) $P_{O_2} = P_{C_2H_4} = 13.3$ kPa.

low pressures to very high pressures as known experimentally. The reaction orders in ethylene vary from 1.0 to −2.0 when ethylene pressure is varied from low to high pressures consistent with experiments. The idea that large variations in reaction orders with varying reaction conditions are due to a change in mechanism is wrong as even simple mechanisms with only one rate-limiting step may display drastic variations in reaction orders. In the case of ethylene oxidation the degree of rate control for steps 2 and 5 does shift with reaction conditions. However, this actually softens the changes in reaction orders. If step 2 was equilibrated instead of being rate limiting much more severe variations in reaction orders would be observed.

In Fig. 10 reaction orders in ethylene and oxygen for C_2H_4O and CO_2 formation versus temperature close to industrial conditions are predicted by the model. It is observed that under industrial conditions a positive reaction order in oxygen and a negative reaction order in ethylene are predicted by the model. The reaction orders in oxygen which exceed one according both to experiments and to the model cannot be explained without the active sites being formed from oxygen (surface oxide) unless coverage dependencies on activation energies are included.

4.4. Activation energy

The apparent activation energy may be calculated from [12]

$$H^{\ddagger} = k_B T^2 \frac{\mathrm{d}\ln(R)}{\mathrm{d}T}, \tag{14}$$

where $H^{\ddagger}$ is the apparent activation enthalpy of an overall rate R, T is the absolute temperature and k_B is Boltzmanns constant.

The apparent activation energy varies as a function of reaction conditions. It is therefore important that the reaction conditions are taken into account when activation energies obtained in different experiments are compared. This is almost never done in the literature. Generally, the apparent activation energy consists of the activation barrier of the rate-limiting steps and the heat of reaction for the elementary reactions taken place prior to the rate-limiting step plus the average enthalpy to create the necessary free sites for the rate-limiting steps to occur, i.e., two free sites in this case. Fig. 11 shows the apparent activation energy for ethylene oxide formation versus temperature predicted by the model for high (curve a) and low (curve b) reactant pressures, respectively. Curve a is close to industrial conditions. The apparent activation energy of CO_2 formation is almost identical to the apparent activation energy of C_2H_4O formation and has been excluded from the figure for simplicity. The apparent activation enthalpy has a high value at low temperatures, but decreases with increasing temperature. This effect is due to an increasing number of free sites with temperature and therefore the enthalpy necessary to form free sites decreases with temperature. For similar reasons the apparent activation enthalpy also increases with reactant pressure as observed by comparing curve a and b in Fig. 11. The observed behavior in Fig. 11 has been observed in a number of cases in the literature [6,51]. The behavior depicted in Fig. 11 is not unusual but is expected for all catalytic reactions containing significant changes in the coverage of intermediates with reaction conditions. With this in mind and the fact that apparent activation energies reported in the literature often are fitted to Arrhenius plots over a significant temperature range major uncertainties are expected. At best, reported activation energies should be considered as an average over the investigated temperature range (range of adsorbate coverages). Furthermore, it makes no sense to report experimental activation energies without simultaneously reporting the reaction conditions under which they were obtained.

Table 9 contains a quantitative comparison between model prediction and experimental activation enthalpies on

Table 9
Reported activation energies and model prediction for different catalysts and reaction conditions in differential reactors

Catalyst	P_{O_2} [kPa]	$P_{C_2H_4}$ [kPa]	T [K]	$H^{\ddagger}_{C_2H_4O}$ [kJ/mol]	$H^{\ddagger}_{CO_2}$ [kJ/mol]	Ref.
Ag(110)	20.0	2.7	450	93.7 (67.9)	93.7 (69.0)	[50]
Ag(110)	20.0	2.7	580	22.2 (33.4)	22.2 (40.1)	[50]
Ag(111)	0.7	0.7	500	45.0 (36.1)	50.0 (36.7)	[42]
Ag(111)	20.0	2.7	610	41.5 (36.5)	45.0 (37.1)	[51]
Ag(111)	20.0	2.7	440	72.3 (72.5)	67.6 (68.5)	[51]
Ag(111)	0.27	0.27	550	25.0 (31.9)	33.0 (27.9)	[64]
Ag(111)	0.27	2.0	550	36.0 (34.8)	47.0 (33.3)	[64]
Ag foil	82.5	15.0	540	49.0 (51.5)	49.0 (51.7)	[104]
Ag sponge	8.7	2.7	450	46.9 (58.2)	60.7 (59.1)	[55]
Ag foil	98.0	2.0	540	31.8 (56.5)	39.3 (56.4)	[108]

Activation energies in parentheses are model prediction.

different catalysts and reaction conditions obtained in different laboratories. It is apparent from Table 9 that the model predicts the experimental reported activation enthalpies within experimental uncertainty. More importantly, the model predicts the changes in activation energy with reaction conditions. The activation energies of ethylene oxide and CO_2 formation are almost identical in most cases. These features would be very hard to explain without introducing a common slow reaction step for epoxidation and combustion as pointed out in the work of Campbell and co-workers [50,51,68, and references therein]. Even more interesting Campbell and co-workers found that both epoxidation and combustion activities varied in a similar way with varying chlorine coverage. Note also that Ag(110) has a higher activation energy than the Ag(111) single crystal.

4.5. Selectivity

We have expanded Campbell's [105] definition of the degree of rate control to define the degree of selectivity control ($X_{SC,i}$)

$$X_{SC,i} = \frac{d\ln(S)}{d\ln(k_i)}, \quad K_i = \text{const}, \tag{15}$$

where S is the selectivity [Eq. (10)] and k_i and K_i are the forward rate constant and equilibrium constant of the ith elementary reaction, respectively. It should be stressed that both the degree of rate and the selectivity control are analytical tools that should be calculated for instantaneous reaction conditions. Fig. 12 shows the predicted degree of selectivity control for different elementary reactions as a function of the total pressure at 500 K. Low total pressure reflects many of the kinetic experiments made in differential laboratory reactors while high total pressures reflects industrial conditions.

The selectivity is mainly controlled by the branching ratio of the oxametallacycle into ethylene oxide and acetaldehyde after the slow formation of the oxametallacycle; i.e., the selectivity is determined after the rate-limiting steps (step 2 + 5). The branching ratio is close to 50% on unpromoted silver. The large inverse isotope effect [55] is due to

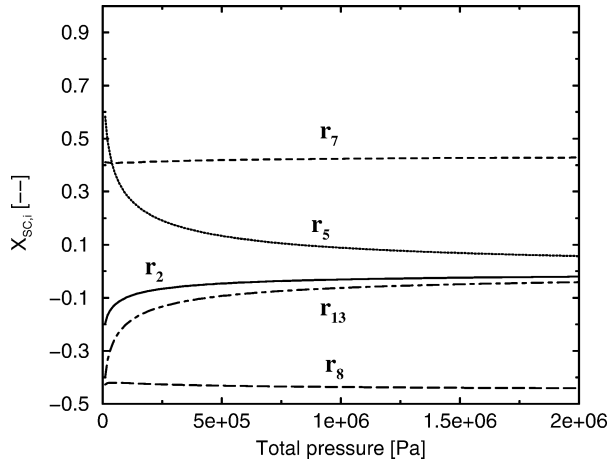

Fig. 12. Degree of selectivity control toward ethylene oxide versus pressure. The feed consists of 90% N_2, 5% O_2, and 5% C_2H_4 at 500 K.

a change in this branching ratio by lowering the rate toward acetaldehyde which needs breaking of a C–H bond. The role of selectivity promoters should also be interpreted as changing the branching pattern of the oxametallacycle. Studying the oxametallacycle is therefore of tremendous importance in understanding the selectivity of ethylene epoxidation. A similar conclusion has been reached by Barteau et al. who studied the oxametallacycle by both experiment and DFT calculations [69,70]. Besides the branching of the oxametallacycle the parallel combustion of ethylene also limits selectivity, cf. Fig. 12. This reaction path is important at low pressures (large numerical values of $X_{SC,5}$ and $X_{SC,13}$), however, saturates quickly in reactant pressures, and become less important at high pressures. This pathway is therefore unimportant under industrial ethylene epoxidation conditions. It is apparent from Fig. 12 that one will obtain very different conclusions for the importance of different elementary reactions if one is studying low or UHV and high-pressure kinetics, respectively.

If the parallel combustion of ethylene through a vinyl alcohol is excluded from the model, a selectivity of ∼55% will be predicted in the limit of zero conversion. In reality the selectivity is lower than 55% except at high oxygen and ethylene pressures due to the parallel combustion.

As observed in Figs. 2 and 3 both the model and the experiments show that selectivity increases with both oxygen and ethylene pressure. The branching ratio of the oxametallacycle is not influenced by reactant pressure. The selectivity variations with reactant pressure are due to the parallel combustion of ethylene, which has a high turnover frequency at low pressures compared to the formation of oxametallacycles.

Increasing selectivity with ethylene pressure is in contradiction to some experiments [3,43,60], indicating selectivity increases with a O_2:C_2H_4 ratio. Actually, the model and some experiments [49–51,64] show that the selectivity increases more with ethylene pressure than oxygen pressure. This paradox is probably not due to a failure of the model

rather it is due to the experimental conditions used in the referenced work. Many of the experiments are transient and it is obvious that oxygen promotes selectivity in such a case because the selective reaction takes place on surface oxide. Another difference is that the model in this work has only been applied on initial conditions while many of the experiments in the literature have a significant conversion. The combustion of the formed ethylene oxide could therefore become important. Finally, many of the catalysts used in the literature are promoted by alkali and/or chlorine either intentionally or due to impurities in the preparation and reactor feed. The model predicts a selectivity of about 20% at low oxygen and ethylene pressures increasing to about 55% at high oxygen/ethylene pressure. This corresponds well to the selectivity reported for unpromoted catalysts in the literature [3, and references therein]. In some cases selectivities as high as 65% have been reported at high reactant pressures [3, and references therein]. This could be due to unintentional promotion by impurities or it could be a real effect missed by the model. There are some indications that the model predicts a too high selectivity at low pressures and a too low selectivity at high pressures. It is important to note, however, that the model predicts the correct selectivity trends. If the model has a serious problem in quantitative prediction of the selectivity it is probably due to the very speculative parallel combustion mechanism of ethylene by nucleophilic oxygen through a vinyl alcohol.

The temperature dependence of the selectivity is more or less constant according to the model which is consistent with some experiments [4,50,51]. However, other experiments indicate that the selectivity decreases with temperature [3, and references therein]. Again the reason for this discrepancy should probably be found in the differences in reaction conditions.

4.6. Critical parameters

The microkinetic model contains a vast number of parameters (Tables 5–8); however, only a small fraction of these are important or critical. The Arrhenius parameter of steps 2, 5, 7, 8, and 13 are of course critical while the Arrhenius parameters of all the remaining steps are uncritical. The stability (enthalpy and entropy) of O^*, O/O^*, C_2H_4/O^*, CH_2CH_2O/O^*, and $C_2H_4^*$ are critical while the stabilities of the remaining intermediates are unimportant. The stability of C_2H_4O/O^*, CO_2^*/CO_3^*, and OH^* might become critical in the presence of reaction products and lead to product inhibition. Product inhibition has been neglected in the present work by analyzing initial rates exclusively. The stability of O^* is uncritical except at very high temperatures; i.e., the formation of surface oxide is determined by kinetics not thermodynamics. The stabilities of O/O^* and C_2H_4/O^* are critical to the formation of the oxametallacycle and site blocking. CH_2CH_2O/O^* is only critical to the further oxidation of ethylene oxide. $C_2H_4^*$ does not participate in any reactions in the model, but are still critical due to site blocking especially under conditions were the oxide coverage θ_{oxide} is low. Under industrial conditions the parallel combustion of ethylene can be neglected without a significant loss of information. However, at low pressure the stability of CH_2CHOH/O^* is critical for the parallel combustion of ethylene.

4.7. Uniqueness of silver

There are many reasons that silver is a unique catalyst for ethylene epoxidation. First of all the catalyst must not decompose adsorbed ethylene and/or ethylene oxide by CH activation like VIII metals [36]. Secondly, ethylene is π-bonded to silver and the double bond is therefore readily accessible for reaction. On other metals such as Pt, Ni, Co, W, and Ru ethylene adsorbs in the di-σ configuration [102]. The catalyst also needs to form a special kind of oxygen (O/O^*) that reacts with the double bond without breaking the single bonds. Silver is able to form this oxygen at high oxygen coverages in our model by creating a surface oxide. Mavrikakis et al. [101] studied the stability of oxametallacycles compared to gaseous ethylene oxide by DFT on 14 different transition metals (groups VIIIa–c, Ib, IIb) and suggested that silver is a unique material, because a moderately stable oxametallacycle is formed on silver. Finally and maybe the most important reason for the uniqueness of silver is the favorable branching ratio of the oxametallacycle. If other catalysts are able to create the oxametallacycle it is very likely that the branching ratio is very unfavorable. Changing H with D in ethylene is enough to significantly change the branching ratio; i.e., changing the catalyst compound could be even more severe. Copper has many of the same features as silver in that atomic oxygen can be formed and ethylene adsorbs by π-bonding. Lambert et al. [13,14] investigated the epoxidation of styrene on Cu(110) and Cu(111) in UHV and found that copper is an even better epoxidation catalyst than silver under UHV conditions. Unfortunately, in the presence of an oxygen atmosphere a stabile surface oxide is formed which poisons the catalyst.

4.8. Other successful models?

The presented model is very complex and even though it is consistent with surface science one could question its validity. The most speculative part is the formation of electrophilic oxygen (O/O^*) on a surface oxide formed by O^*. One might argue that subsurface oxygen creates the electrophilic oxygen instead. It is not possible to study the electrophilic oxygen directly in UHV. However, whether our conjecture is true or not the present model explains ethylene epoxidation very well and it pinpoints all the features a successful model should contain. In a successful model the active sites should be created by oxygen and the active oxygen should be adsorbed on these sites together with ethylene

which reacts in a slow step forming a common intermediate for both epoxidation and combustion.

Linic and Barteau [71] suggested a much more simple microkinetic model based on first principles. The model was evaluated against apparent activation energies and reaction orders of ethylene and oxygen [71]. We compared the output of the Linic and Barteau model to the Ag(111) steady-state kinetics depicted in Figs. 1–3 and found that the model underestimates the activity by almost two orders of magnitude. However, interestingly both the microkinetic model developed in this work and the model of Linic and Barteau [69,71] suggests that both the uptake of atomic surface oxygen and the surface reaction between adsorbed ethylene and atomic oxygen are rate limiting. Further, the selectivity is determined by the branching ratio of the oxametallacycle in both models. Actually, the present model agrees with the work of Linic and Barteau regarding all aspects of importance to industrial ethylene epoxidation. However, it disagrees on the very important academic question, what is the active phase of the catalyst and the active oxygen species in epoxidation.

5. Conclusion

In the present work a detailed microkinetic model of ethylene oxidation on silver based on surface science has been developed. The reaction mechanism and model parameters have been deduced from surface science experiments mostly on Ag(111) and steady-state kinetics on Ag(111). The important idea in this model is that a surface oxide (/O*) is created supplying the active sites for adsorption of ethylene and electrophilic oxygen (O/O*), which reacts to form an oxametallacycle. The oxametallacycle is a common intermediate for ethylene epoxidation, ethylene combustion, and ethylene oxide combustion. Furthermore, a parallel combustion route of ethylene by O* exists, which is of minor importance except at low pressures. The idea of a formation of an active oxide layer and a common intermediate has been suggested earlier in the literature in different contexts. The overall activity is mainly determined by the rate of formation of the oxide layer (step 2) and oxametallacycle (step 5). The selectivity is mainly determined by the branching ratio of the oxametallacycle into ethylene oxide and acetaldehyde, respectively. At low pressures the parallel combustion of ethylene (step 13) also influences activity and selectivity. Changes in the branching ratio of the oxametallacycle explain the large inverse isotope effect on selectivity observed when ethylene is substituted with deuterated ethylene. The role of selectivity promoters is also to change the branching ratio of the oxametallacycle either by electronic or by structural effects.

The values of the parameters of the model are physically and chemically realistic and the model predicts heat of adsorption, sticking, TPD, and TPR measurements. In short the model reproduces a broad range of transient surface science experiments. The model explains the kinetics of epoxidation, ethylene combustion, and ethylene oxide combustion. The model has been validated by comparing model output to measured initial rates on a variety of catalysts for both ethylene- and oxygen-rich mixtures at different temperatures. From this it is clear that the mechanism remains the same on different unpromoted silver catalysts; however, large changes in site densities occur. The large variations in ethylene and oxygen reaction orders and apparent activation energies observed experimentally are captured by the model. Furthermore, the trends in selectivity variations with reaction conditions are predicted by the model.

The great success of the model in predicting both surface science and kinetic experiments demonstrates that the microkinetic model contains the essential physics and chemistry to explain ethylene oxidation on silver. It is possible even likely that the model needs adjustments concerning parameters and elementary reactions as a consequence of future experimental and theoretical progress. Especially, the oxygen–silver system is very complex and speculative and may need adjustments in the future. However, the main structure and conclusions of the model will prevail in our view; i.e., oxygen creates the active sites, an active loosely bonded electrophilic oxygen is formed on the active sites, and an oxametallacycle is a common intermediate in both epoxidation and combustion. Unfortunately, it is not possible to obtain an analytic solution of the model.

Acknowledgment

C.T.C. acknowledges the Department of Energy, Office of Basic Energy Sciences, Chemical Sciences Division for partial support of this work.

References

[1] C.N. Satterfield, Heterogeneous Catalysis, 2nd ed., McGraw–Hill, New York, 1991.
[2] Ullmann's Encyclopedia of Industrial Chemistry, 5th ed., Vol. A11, VCH, 1988.
[3] R.A. van Santen, H.P.C.E. Kuipers, Adv. Catal. 35 (1987) 265–321.
[4] H.R. Dettwiler, A. Baiker, W. Richarz, Helv. Chim. Acta 62 (1979) 1689–1700.
[5] L. Petrov, A. Eliyas, C. Maximov, D. Shopov, Appl. Catal. 41 (1988) 23–38.
[6] G.H. Twigg, Proc. R. Soc. A 188 (1946) 92–141.
[7] G.H. Twigg, Trans. Faraday Soc. 42 (1946) 284–294.
[8] H. Takada, Shokubai 38 (1996) 213–217.
[9] P.A. Kilty, W.M.H. Sachtler, Catal. Rev.-Sci. Eng. 10 (1974) 1–16.
[10] J.G. Serafin, A.C. Liu, S.R. Seyedmonir, J. Mol. Catal. A: Chem. 131 (1998) 157–168.
[11] J. Dumesic, D. Rudd, L. Aparicio, J. Rekoske, A. Treviño, The Microkinetics of Heterogeneous Catalysis, Am. Chem. Society, Washington, DC, 1993.
[12] P. Stoltze, Prog. Surf. Sci. 65 (2000) 65–100.
[13] J.J. Cowell, A.K. Santra, R. Lindsay, R.M. Lambert, A. Baraldi, A. Goldoni, Surf. Sci. 437 (1999) 1–8.

[14] A.K. Santra, J.J. Cowell, R.M. Lambert, Catal. Lett. 67 (2000) 87–91.
[15] J.W. Medlin, M.A. Barteau, J.M. Vohs, J. Mol. Catal. A 163 (2000) 129–145.
[16] J.W. Medlin, J.R. Monnier, M.A. Barteau, J. Catal. 204 (2001) 71–76.
[17] J.R. Monnier, J.W. Medlin, M.A. Barteau, J. Catal. 203 (2001) 362–368.
[18] S. Hawker, C. Mukoid, J.P.S. Badyal, R.M. Lambert, Surf. Sci. 219 (1989) L615–L622.
[19] B.S. Bal'zhinimaev, Kinet. Catal. 40 (1999) 795–810.
[20] C.T. Campbell, Surf. Sci. 157 (1985) 43–60.
[21] C.T. Campbell, Surf. Sci. 173 (1986) L641–L646.
[22] A. Raukema, D.A. Butler, F.M.A. Box, A.W. Kleyn, Surf. Sci. 347 (1996) 151–168.
[23] S.R. Bare, K. Griffiths, W.N. Lennard, H.T. Tang, Surf. Sci. 342 (1995) 185–198.
[24] R.B. Grant, R.M. Lambert, Surf. Sci. 146 (1984) 256–268.
[25] M. Dean, M. Bowker, Appl. Surf. Sci. 35 (1988–1989) 27–40.
[26] C.I. Carlisle, D.A. King, M.L. Bocquet, J. Cerda, P. Sautet, Phys. Rev. Lett. 84 (2000) 3899–3902.
[27] C.I. Carlisle, T. Fujimoto, W.S. Sim, D.A. King, Surf. Sci. 470 (2000) 15–31.
[28] C. Backx, J. Moolhuysen, P. Geenen, R.A. van Santen, J. Catal. 72 (1981) 364–368.
[29] R.A. van Santen, C.P.M. de Groot, J. Catal. 98 (1986) 530–539.
[30] X. Bao, M. Muhler, Th. Schedel-Niedrig, R. Schlögl, Phys. Rev. B 54 (1996) 2249–2262.
[31] D. Stacchiola, G. Wu, M. Kaltchev, W.T. Tysoe, Surf. Sci. 486 (2001) 9–23.
[32] C. Backx, C.P.M. de Groot, P. Biloen, W.M.H. Sachtler, Surf. Sci. 128 (1983) 81–103.
[33] B. Krüger, C. Benndorf, Surf. Sci. 178 (1986) 704–715.
[34] C. Benndorf, B. Krüger, B. Nieber, Appl. Catal. 25 (1986) 165–172.
[35] S.R. Bare, J. Vac. Sci. Technol. A 10 (1992) 2336–2341.
[36] C.T. Campbell, M.T. Paffett, Surf. Sci. 177 (1986) 417–430.
[37] G. Wu, D. Stacchiola, M. Collins, W.T. Tysoe, Surf. Rev. Lett. 7 (2000) 271–275.
[38] E.M. Stuve, R.J. Madix, B.A. Sexton, Surf. Sci. 111 (1981) 11–25.
[39] C.T. Campbell, M.T. Paffett, Surf. Sci. 143 (1984) 517–535.
[40] G.S. Jones, M. Mavrikakis, M.A. Barteau, J.M. Vohs, J. Am. Chem. Soc. 120 (1998) 3196–3204.
[41] G. Wu, D. Stacchiola, M. Kaltchev, W.T. Tysoe, Surf. Sci. 463 (2000) 81–92.
[42] R.B. Grant, R.M. Lambert, J. Catal. 92 (1985) 364–375.
[43] R. Haul, G. Neubauer, J. Catal. 105 (1987) 39–54.
[44] V.I. Bukhtiyarov, A.I. Boronin, V.I. Savchenko, J. Catal. 150 (1994) 262–267.
[45] S. Kagawa, M. Iwamoto, H. Mori, T. Seiyama, J. Phys. Chem. 85 (1981) 434–439.
[46] C. Henriques, M.F. Portela, C. Mazzocchia, in: V.C. Corberan, S.V. Bellon (Eds.), New Developments in Selective Oxidation II, Elsevier Science, Amsterdam, 1994, pp. 499–506.
[47] J.T. Gleaves, A.G. Sault, R.J. Madix, J.R. Ebner, J. Catal. 121 (1990) 202–218.
[48] J. Mikami, S. Satoh, H. Kobayashi, J. Catal. 18 (1970) 265–270.
[49] S.L. Guseinov, I.T. Frolkina, L.A. Vasilevich, A.K. Avetisov, A.I. Gel'bshtein, Kinet. Katal. 18 (1977) 1455–1462.
[50] C.T. Campbell, M.T. Paffett, Surf. Sci. 139 (1984) 396–416.
[51] C.T. Campbell, J. Catal. 94 (1985) 436–444.
[52] R.B. Grant, R.M. Lambert, J. Catal. 93 (1985) 92–99.
[53] P.L. Metcalf, P. Harriott, Ind. Eng. Chem. Proc. Des. Dev. 11 (1972) 478–484.
[54] P.D. Klugherz, P. Harriott, AIChE J. 17 (1971) 856–866.
[55] N.W. Cant, W.K. Hall, J. Catal. 52 (1978) 81–94.
[56] L.G. Nault, D.W. Bolme, L.N. Johanson, I&EC Proc. Des. Dev. 1 (1962) 285–292.
[57] R.E. Kenson, M. Lapkin, J. Phys. Chem. 74 (1970) 1493–1502.
[58] A. Orzechowski, K.E. MacCormack, Can. J. Chem. 32 (1954) 388–451.
[59] D. Lafarga, M.A. Al-Juaied, C.M. Bondy, A. Varma, Ind. Eng. Chem. Res. 39 (2000) 2148–2156.
[60] L. Petrov, A. Eliyas, D. Shopov, Appl. Catal. 18 (1985) 87–103.
[61] E.L. Force, A.T. Bell, J. Catal. 40 (1975) 356–371.
[62] M.I. Temkin, Adv. Catal. 28 (1979) 173–291.
[63] X.E. Verykios, F.P. Stein, R.W. Coughlin, Catal. Rev.-Sci. Eng. 22 (1980) 197–234.
[64] S.A. Tan, R.B. Grant, R.M. Lambert, Appl. Catal. 31 (1987) 159–177.
[65] H.H. Voge, C.R. Adams, Adv. Catal. 17 (1967) 151–221.
[66] C.T. Campbell, M.T. Paffett, Appl. Surf. Sci. 19 (1984) 28–42.
[67] C.T. Campbell, B.E. Koel, J. Catal. 92 (1985) 272–283.
[68] C.T. Campbell, J. Catal. 99 (1986) 28–38.
[69] S. Linic, M.A. Barteau, J. Am. Chem. Soc. 125 (2003) 4034–4035.
[70] S. Linic, M.A. Barteau, J. Am. Chem. Soc. 124 (2002) 310–317.
[71] S. Linic, M.A. Barteau, J. Catal. (2003) 200–212.
[72] M.L. Bocquet, A. Michaelides, D. Loffreda, P. Sautet, A. Alavi, D.A. King, J. Am. Chem. Soc. 125 (2003) 5620–5621.
[73] E.A. Carter, W.A. Goddard III, Surf. Sci. 209 (1989) 243–289.
[74] A. Andreasen, H. Lynggaard, C. Stegelmann, P. Stoltze, Surf. Sci. 544 (2003) 5–23.
[75] R.D. Cortright, J.A. Dumesic, Adv. Catal. 46 (2001) 161–264.
[76] P. Stoltze, Phys. Scr. 36 (1987) 824–864.
[77] C.V. Ovesen, B.S. Clausen, B.S. Hammershøi, G. Steffensen, T. Askgaard, I. Chorkendorff, J.K. Nørskov, P.B. Rasmussen, P. Stoltze, P. Taylor, J. Catal. 158 (1996) 170–180.
[78] T.S. Askgaard, J.K. Nørskov, C.V. Ovesen, P. Stoltze, J. Catal. 156 (1995) 229–242.
[79] C.T. Campbell, Top. Catal. 1 (1994) 353–366.
[80] V.P. Zhdanov, B. Kasemo, Surf. Sci. Rep. 20 (1994) 113–189.
[81] S.H. Oh, G.B. Fisher, J.E. Carpenter, D.W. Goodman, J. Catal. 100 (1986) 360–376.
[82] N. Waletzko, L.D. Schmidt, AIChE J. 34 (1988) 1146–1156.
[83] D.A. Hickman, L.D. Schmidt, AIChE J. 39 (1993) 1164–1177.
[84] C. Stegelmann, P. Stoltze, in preparation.
[85] A. Michaelides, M.L. Bocquet, P. Sautet, A. Alavi, D.A. King, Chem. Phys. Lett. 367 (2003) 344–350.
[86] W.-X. Li, C. Stampfl, M. Scheffler, Phys. Rev. B 67 (2003) 045408.
[87] W.-X. Li, C. Stampfl, M. Scheffler, submitted for publication.
[88] V.I. Bukhtiyarov, V.V. Kaichev, I.P. Prosvirin, J. Chem. Phys. 111 (1999) 2169–2175.
[89] E.L. Force, A.T. Bell, J. Catal. 38 (1975) 440–460.
[90] W.M.H. Sachtler, C. Backx, R.A. van Santen, Catal. Rev.-Sci. Eng. 23 (1981) 127–149.
[91] M.L. Bocquet, P. Sautet, J. Cerda, C.I. Carlisle, M.J. Webb, D.A. King, J. Am. Chem. Soc. 125 (2003) 3119–3125.
[92] A.W. Czanderna, J. Vac. Sci. Technol. 14 (1977) 408–411.
[93] M.A. Barteau, R. Madix, in: D.A. King, B.P. Woodruff (Eds.), The Chemical Physics of Solid Surfaces and Heterogeneous Catalysis, vol. 4, Elsevier, Amsterdam, 1982, pp. 95–142.
[94] K. Reuter, M. Scheffler, Phys. Rev. Lett. 90 (2003) 046103-1–046103-4.
[95] D.I. Kondarides, X.E. Verykios, J. Catal. 143 (1993) 481–491.
[96] N. Macleod, J.M. Keel, R.M. Lambert, Catal. Lett. 86 (2003) 51–56.
[97] D.J. Sajkowski, M. Boudart, Catal. Rev.-Sci. Eng. 29 (1987) 325–360.
[98] M.W. Chase Jr (Ed.), NIST-JANAF Thermochemical Tables, 4th ed., J. Phys. Chem. Ref. Data, monograph No. 9, Parts I and II.
[99] X.D. Wang, W.T. Tysoe, R.G. Greenler, K. Truszkowska, Surf. Sci. 257 (1991) 335–343.
[100] V.I. Bukhtiyarov, A.I. Boronin, I.P. Prosvirin, V.I. Savchenko, J. Catal. 150 (1994) 268–273.
[101] M. Mavrikakis, D.J. Doren, M.A. Barteau, J. Phys. Chem. B 102 (1998) 394–399.
[102] R.I. Masel, Principles of Adsorption and Reaction on Solid Surfaces, Wiley, 1996.

[103] S.A. Tan, R.B. Grant, R.M. Lambert, J. Catal. 100 (1986) 383–391.
[104] H. Kestenbaum, A.L. de Oliveira, W. Schmidt, F. Schüth, et al., Ind. Eng. Chem. Res. 41 (2002) 710–719.
[105] C.T. Campbell, J. Catal. 204 (2001) 520–524.
[106] C. Backx, C.P.M. de Groot, P. Biloen, Appl. Surf. Sci. 6 (1980) 256–272.
[107] C.G.P.M. Bernardo, J.A.N.F. Gomes, J. Mol. Struct., in press.
[108] L. Imre, Ber. Bunsen-Ges. 74 (1970) 220–226.